AN ABSTRACT OF THE THESIS OF

Colin C. Davis for the degree of Master of Science in Mechanical Engineering presented on June 25, 1996. Title: Modeling the Thermal Inkjet Firing Process.

Abstract approved: Redacted for Privacy

Heidi A. Pattee

A numerical model has been developed to simulate the firing of an inkjet printhead. The model evaluates the heat generation and diffusion within the thin film structure, the phase change and vapor bubble growth in the ink, and the subsequent flow of ink from the orifice. The heat transfer is modeled numerically throughout the printhead's thin film structure and ink through an asymptotic integration algorithm. The bubble growth and fluid flow are coupled and modeled through conservation of momentum, conservation of energy, and state equations.

The heat transfer model has been validated with simple theoretical solutions and ink drop weight and velocity have been compared to empirical data. To test the usefulness of the model as a design tool, parametric studies have been made which characterize pen performance as a function of several system parameters. The results show that although the model does not reflect every detail in the firing process, it is useful for predicting trends and investigating new design concepts.

# Modeling the Thermal Inkjet Firing Process

by

Colin C. Davis

A THESIS

submitted to

Oregon State University

in partial fulfillment of
the requirements for the
degree of

Master of Science

Presented June 25, 1996
Commencement June 1997

Master of Science thesis of Colin C. Davis presented on June 25, 1996

APPROVED:

Redacted for Privacy

Major Professor, representing Mechanical Engineering

Redacted for Privacy

Chair of Department of Mechanical Engineering

Redacted for Privacy

Dean of Graduate School

I understand that my thesis will become part of the permanent collection of Oregon State University libraries. My signature below authorizes release of my thesis to any reader upon request.

Redacted for Privacy

Colin C. Davis, Author

## ACKNOWLEDGEMENT

The author would like to thank the Hewlett Packard inkjet research group for the opportunity to work on this project and for the help and advice they provided. I would also like to thank professor Heidi Pattee for all the guidance and direction she provided during the course of this research. Professor Pattee deserves special credit for her effort in assuring that my graduate career was complete through her weekly research meetings and ski trips.

My family deserves much credit for their motivation and support during my academic career. Last, I thank my wife without whose love and support I would have not gone to graduate school at all.

# TABLE OF CONTENTS


INTRODUCTION ..... 1

Project Overview ..... 1

Background ..... 1

Vapor Nucleation and Growth ..... 4

Project Approach ..... 6

MODEL DEVELOPMENT ..... 8

Heat Conduction ..... 9

Bubble Nucleation and Growth ..... 12

Equation of Motion ..... 13

Energy Conservation ..... 14

State Equation ..... 18

Ink Chamber Refill ..... 19

Numerical Implementation ..... 20

CODE VALIDATION ..... 27

Theoritical Comparison ..... 27

Error Testing on Actual Geometry ..... 29

RESULTS ..... 33

Thermal Characteristics of the Structure ..... 33

Bubble Characteristics ..... 37

Parametric Studies ..... 38

Predicting Turn On Curves ..... 44

CONCLUSION ..... 50

BIBLIOGRAPHY ..... 53

# LIST OF FIGURES


| Figure | | Page |
|---|---|---|
| 1.1 | Firing chamber side view | 2 |
| 2.1 | Model boundary | 8 |
| 2.2 | Heat transfer coefficients on corresponding face of a 3-D node | 10 |
| 2.3 | Example of overall heat transfer coefficient calculation | 11 |
| 2.4 | Solution domain for heat conduction above bubble surface | 16 |
| 2.5 | Spherical cap geometry | 17 |
| 2.6 | Bubble shape modeled as spherical cap | 18 |
| 2.7 | Actual and modeled nozzle shape | 21 |
| 2.8 | Program flowchart for one time step | 23 |
| 2.9 | Ghost node example | 25 |
| 3.1 | Comparison of exact and numerical solutions for different grid sizes | 28 |
| 3.2 | Comparison of exact and numerical solutions for different time step values | 29 |
| 3.3 | Model geometry | 30 |
| 3.4 | Material data from Knight, Clark | 31 |
| 3.5 | Global numerical error versus time step | 32 |
| 4.1 | Heater surface temperature for three pulses | 34 |
| 4.2 | High resolution heater surface temperature for one pulse | 34 |
| 4.3 | Temperature profile in the thin film structure at the time of nucleation | 35 |
| 4.4 | Printhead energy distribution at time of nucleation | 36 |
| 4.5 | The bubble growth process | 37 |
| 4.6 | Pressure history for the life of the vapor bubble | 38 |
| 4.7 | Parameter variations | 40 |
| 4.8 | Main effects plot. Individual parameter effects on efficiency | 41 |
| 4.9 | Parameter interaction plot | 43 |
| 4.10 | Typical turn-on curve for a printhead | 44 |
| 4.11 | Numerical and experimental turn-on curves | 46 |

## LIST OF FIGURES (CONTINUED)


| Figure | | Page |
|---|---|---|
| 4.12 | Drop velocities versus input energy | 47 |
| 4.13 | Experimental drop masses for two pulse delay times | 48 |
| 4.14 | Numerical drop masses for two delay times | 48 |

# NOMENCLATURE

| | |
|---|---|
| A | area |
| Bubb | bubble |
| Cp | specific heat |
| E | energy |
| h | convective heat transfer coefficient or spherical cap height or enthalpy |
| k | thermal conductivity |
| M | inertance factor |
| m | mass |
| P | pressure |
| q" | heat flux |
| Q''' | volumetric heat generation |
| r | sperical radius |
| T | temperature |
| t | time |
| U | overall heat transfer coefficient |
| V | asymptotic integration algorithm coefficient |
| Vol | volume |
| W | asymptotic integration algorithm coefficient |
| x, y, z | directions in the rectangular coordinate system |

## NOMENCLATURE (CONTINUED)

Greek

| | |
|---|---|
| $\alpha$ | thermal diffusivity |
| $\Delta$ | discrete step in time or space |
| $\upsilon$ | specific volume |
| $\rho$ | density |

Subscripts

| | |
|---|---|
| atm | atmospheric |
| f | fluid |
| fg | transition from liquid to gaseous state |
| i | nodal index in the x-direction |
| j | nodal index in the y-direction |
| k | nodal index in the z-direction |
| v | vapor |
| sat | saturation |

Superscript

| | |
|---|---|
| n | time step index |

Modeling the Thermal Inkjet Firing Process

# INTRODUCTION

## Project Overview

A numerical model has been developed to simulate the firing of an inkjet printhead. The model evaluates the heat generation and diffusion within the thin film structure, the phase change and vapor bubble growth in the ink, and the subsequent flow of ink from the orifice. The heat transfer model has been validated with simple theoretical solutions and ink drop weight and velocity have been compared to empirical data. To test the usefulness of the model as a design tool, parametric studies have been made which characterize pen performance as a function of several system parameters.

## Background

Inkjet printer technology allows high resolution color printing from the ejection of micro-scale ink drops of different colors onto paper. The ink drops are ejected from printheads containing over 100 microscopic firing chambers; these chambers are connected to a common ink supply bladder. The ink drop ejection is made possible through the use of high pressure generators within the firing chamber controlled by voltage signals sent from the printer's software (Asai 1987). These pressure generators can take the form of small piezoelectric devices or high pressure vapor bubbles in the ink, each having its advantages. Piezoelectric transducers are an established technology able to

produce ink drops at predictable times but their size limits the orifice size and nozzle spacing, directly affecting print resolution (Asai 1987). Microscopic, high pressure vapor bubbles can be grown through the use of high heat fluxes generated with a thin film resistor placed at the nozzle. Inkjet printers that use this method of drop ejection are called thermal inkjets or bubble jets, and are preferred over piezoelectric devices due to their ability to accommodate smaller firing nozzles and multi-nozzle printheads.

The thin film resistor used to produce the heat fluxes required for bubble formation is produced in much the same way integrated circuits are fabricated (Bhaskar 1985). Thin films of different materials are sputter deposited onto a structural substrate, usually silicon, which produces an electrical conductor and a resistor to generate heat among other layers, each with its own purpose. A typical printhead structure resulting from this process is shown in Fig. 1.1, which shows a two-dimensional view of one firing chamber.

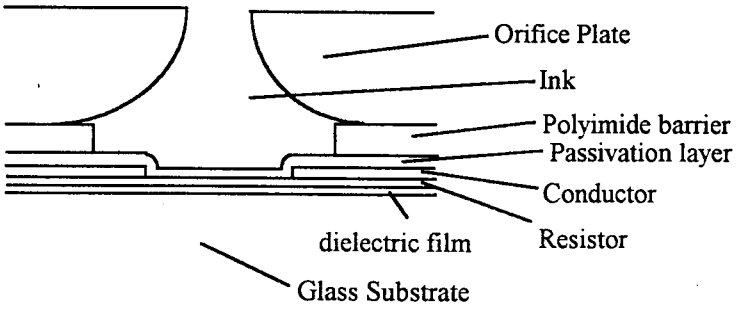


Figure 1.1 - Firing chamber side view

The dielectric film shown in Fig. 1.1 is usually a silicon oxide, and is used to prevent leaching of impurities from the substrate into the upper layers. On top of the dielectric film, the resistor (Ta alloy) and an aluminum conductor are deposited and the conductor is etched away above the resistor, forcing an electrical current path through the resistor and forming the step shown in Fig. 1.1. Finally, passivation layers are deposited to protect the

conductor and resistor from chemical attack by the ink and the destructive action of bubble collapse (Asai 1987, Bhaskar 1985). The entire thin film structure is built on top of the substrate and is less than 4 μm thick (Patzer 1994). Above the thin film stack lies a polyimide barrier layer and an orifice plate, which form an ink chamber. When an ink droplet is fired, an electric current is passed through the resistor to generate heat. This heat is diffused across the whole structure and heats the ink to nucleation within a few microseconds. Once nucleation has occurred, a vapor bubble grows rapidly on the surface of the passivation layers, forcing ink through the orifice plate and onto paper. The bubble eventually cools to the point of collapse and the ink chamber is refilled through surface tension effects.

Since an image may consist of millions of ink drops, inkjets must be able to rapidly deposit ink drops precisely in time and space. Therefore, the firing process must be very reliable and predictable. Also, since the drop ejection is just one part of many mechanical events necessary to produce an image, the ejection must take place on the order of microseconds. These criteria require a predictable and repeatable firing mechanism to ensure quality printing (Bohorquez 1994). The main disadvantage of thermal inkjets is the unpredictable nature of vapor generation and bubble growth. The high frequency (4000 Hz) heating and cooling cycles necessary to eject the millions of drops needed for an image, result in large cyclic temperature gradients. These gradients combined with the different coefficients of thermal expansion among the thin film layers contribute to thermal stresses in the thin film structure, creating another mode of failure (Allen 1985).

To improve the reliability of bubble formation and to ensure that the printhead's life exceeds that of the ink supply, control of the thermal energy supplied through the resistor is crucial. Ideally, all the supplied thermal energy would be converted directly into the ink drop's kinetic energy. In reality, the thermal energy diffuses across the whole thin film structure. This thermal spreading causes uncertainties in the heat flux applied to the ink and decreases efficiency. This displaced thermal energy is also the cause of thermal stresses within the structure.

To decrease uncertainties when firing an inkjet printer, it is important to understand and predict the underlying thermal mechanisms at work. Previous numerical

studies of inkjet printing have concentrated primarily on the fluid dynamics of the ink as it moves through the nozzle during firing (Allen 1985, Knight 1991, Elger 1986). Also, Asai (1987, 1989, 1991) has done extensive work on nucleation mechanisms and bubble growth under high heat flux heating environments encountered in thermal inkjets. Patzer (1994), studied the influence of different types of inks on the thermodynamics of a firing inkjet. He used a commercial code to combine a three-dimensional heat transfer model of the thin film structure with that of bubble growth to try to accurately describe the thermal behavior of these devices during firing.

## Vapor Nucleation and Growth

Since repeatability is so important in producing ink drops, it is very important to understand the vapor nucleation and bubble growth mechanisms that take place in firing a thermal inkjet. Vapor formation can fit into two general categories: homogeneous and heterogeneous nucleation. Nucleation is a term used to describe any discontinuous change of phase (Michaels 1966). The term nucleation, in this thesis, refers to the change in phase from liquid to vapor.

Heterogeneous nucleation occurs at a solid/fluid interface and is strongly dependent on the physical conditions and properties of that interface. Important interface conditions that influence this type of nucleation include the presence of small pits, imperfections, and trapped vapor. These contaminations provide nucleation sites, and preexisting nuclei in which a bubble can start (Hsu 1976). Heterogeneous nucleation is the most common mechanism in everyday boiling, where vapor forms with small amounts of superheat. This type of boiling is undesirable in producing an ink drop since inkjet printheads produce up to 4000 vapor bubbles per second, resulting in changes in the heater surface over time. Also, after a few firings vapor can become trapped on the surface, providing additional nucleation sites. This uncertainty in determining surface/fluid

interface conditions causes bubble formation by this mechanism to be uncertain and could cause inconsistencies in bubble formation from firing to firing.

Homogeneous nucleation occurs within the bulk of the fluid and is independent of surface conditions. Homogenous nucleation is caused by thermal fluctuations in molecular density and occurs at extreme superheated nonequilibrium temperatures (Michaels 1965). This type of boiling is also known as spontaneous nucleation since vapor nuclei are spontaneously formed in the liquid (Asai 1989). Homogeneous nucleation is usually not observed since conventional boiling occurs through heterogeneous nucleation at low levels of superheat on container walls (Michaels 1966). In order for homogeneous boiling to occur, very high heat fluxes are needed to produce these spontaneous nuclei before the growth of pre-existing nuclei (heterogeneous nucleation) has time to take place. The goal of vapor formation and vapor bubble growth in thermal inkjets is to bypass any dependence of surface conditions and to rely solely on spontaneous nucleation for better repeatability. Because of the high superheated temperatures at which homogeneous nucleation occurs the vapor pressure is also very high, producing a faster drop ejection than could be obtained with heterogeneous nucleation.

The advantages that homogeneous nucleation offers in reliability are offset somewhat by increased modeling complexity. In order to model homogeneous boiling, knowledge is needed of typical nucleation temperatures under the high heat flux conditions present in an inkjet chamber ($500 \frac{MW}{m^2}$, Allen 1985). Also, bubble growth under these high superheat, nonequilibrium conditions is not well understood.

Two approaches have been used in the literature to estimate this homogenous nucleation point for inkjet modeling. One approach is to use a stochastic model based on classical nucleation theory (Asai 1989). This method takes the random nature of nucleation into account and determines the probability of spontaneous and heterogeneous nucleation as the ink is heated over time. Using a numerical approach, the nucleation probability is determined at each discrete time step and then the actual occurrence of nucleation is checked using numerically generated random numbers. This is a rigorous approach since both heterogeneous and homogeneous mechanisms are taken into consideration.

A simpler approach is to use a deterministic criterion for bubble nucleation (Allen 1985, Runge 1993), disregarding any low temperature nucleation sites. This approach sets a temperature ceiling above which homogenous nucleation is assumed to occur. This temperature limit can either be specified from empirical data or taken as the superheat limit of the fluid.

Once vapor nucleation has occurred, some scheme has to be used to track the growth of the vapor bubble. Several attempts have been made to model the bubble growth process mathematically. Plesset and Zwick (1954) calculated the growth of a spherical bubble under low superheat conditions. They used an analytical expression to represent the conduction of the superheated thermal layer outside the bubble, an energy balance at the bubble/liquid interface, and an equation of motion to describe the inertia of fluid around the bubble. With this, they were able to link the dynamic problem of bubble growth with a heat diffusion problem. Florschuetz (1965) studied the mechanisms of bubble collapse, also using the coupled effects of liquid inertia and heat transfer from liquid to bubble. Asai (1987) coupled the energy balance across the bubble surface with the bubble growth in order to model drop ejection from a thermal inkjet device. Asai's work assumes a rectangular bubble shape and a heat flux at the heater surface which does not consider the heat diffusion process across the entire thin film structure. The bubble pressure needed for the equations of motion is most often modeled through the Clausius-Clapeyron equation (Allen (1985), Asai (1987), Patzer (1994)).

## Project Approach

The objective of the current study was to model the important processes that take place in firing an inkjet printhead. This model provides a tool for use in predicting pen performance and to help in future inkjet design. The model also made predicting the energy distribution in the thin film structure and calculation of the thermal efficiency of

the system for a printhead possible. The model was also used to study the effect of varying system parameters on the thermal efficiency. Thermal efficiency in this case was defined as the kinetic energy of the ink drop ejected from the head divided by the amount of energy supplied through the resistor. These objectives were accomplished by modeling the heat transfer in the structure, the vapor nucleation and bubble growth, and the bulk fluid flow through the ink chamber and nozzle. Additionally, it was desired to create a computationally economic solution scheme which would use a fraction of the computational time usually required for such complex simulations.

This study incorporated a three part approach: building of the numerical model, model validation, and producing results used to describe the behavior of the firing process. The last step included performing parametric studies to characterize pen performance as a function of important system variables.

The model development phase consisted of gaining an understanding of the mechanisms that take place in firing a thermal inkjet and deciding what assumptions to make. The important mechanisms considered include three dimensional transient heat conduction in the composite structure, vapor bubble nucleation and growth, and the subsequent drop ejection.

During and after the model building process, different means of code validation were performed. Validation included comparisons to exact solutions of simple theoretical heat conduction cases, optimization of the effect of time and spatial step sizes, and comparison of numerical results to experimental results.

Once the model was built, results were produced to describe the behavior of the firing process. These results included temperature and energy distributions, bubble properties, and drop volume and speed. A numerical parametric study was conducted on select system variables to observe their effect on the thermal efficiency. A partial factorial experimental design based on the Box-Behnken factorial method (Box 1960) was used to study the interdependency of the system variables.

# MODEL DEVELOPMENT

This chapter describes the mathematical development and numerical implementation of the model used to simulate the firing of an inkjet. The model is based on the geometry and operation of a typical printhead nozzle as shown by the two-dimensional slice of the composite structure and ink chamber in Fig. 2.1. This figure also shows the model boundaries, where the solution domain does not exceed the step caused by the aluminum conductor.

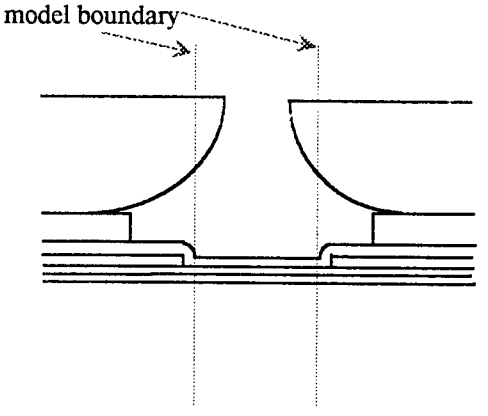


Figure 2.1-Model Boundary

The operation of an inkjet nozzle involves three distinct steps for each firing: 1) heat generation in the thin film resistor and the subsequent heat diffusion in the structure and ink before bubble nucleation occurs; 2) growth and collapse of the vapor bubble once nucleation has occurred resulting in an ejection of an ink drop; and 3) refill of the ink chamber and further diffusion of the residual heat in the structure. The model presented includes these three processes and each is described below.

Heat Conduction

The thermal model is represented in three dimensions in order to accurately predict the temperature fields in the structure and liquid, although no attempt to model complex 3-D nozzle geometry was made. Some previous models represented only one dimensional heat transfer in order to reduce model construction and computational time (Allen 1985). One of the goals of this project was to model several consecutive firings, so evaluation of three dimensional heat dissipation mechanisms was necessary. Furthermore, the solution scheme used for solving the temperature fields substantially reduced computational time, making three-dimensional modeling reasonable.

Heat conduction in the thin film structure and ink fluid occurs in all three steps of the inkjet's operation because of the finite temperature differences in the medium. The temperature distributions are solved through the three-dimensional, transient heat conduction equation,

$$\frac{\partial T}{\partial t}\rho C_p = k\left(\frac{\partial^2 T}{\partial x^2} + \frac{\partial^2 T}{\partial y^2} + \frac{\partial^2 T}{\partial z^2}\right) + Q''' \qquad (2.1)$$

assuming that the thermal properties of the structure are independent of temperature and direction. Equation (2.1) was discretized for the domain defined by the model to solve for the temperature distribution in the thin film structure and ink. To account for the different material thicknesses and properties in the structure, each node is assigned its own volume, mass and physical properties and communicates with each of its neighboring nodes. To solve for the nodal temperatures at each time step, the spatial derivatives in equation (2.1) were discretized to give equation (2.2).

$$\frac{\partial T}{\partial t}(mC_p)_{ijk} = \dot{Q}_{ijk} + U_1A_1(T_{i,j,k+1} - T_{i,j,k}) + U_2A_2(T_{i,j,k-1} - T_{i,j,k}) \qquad (2.2)$$

$$+U_3A_3(T_{i,j+1,k} - T_{i,j,k}) + U_4A_4(T_{i,j-1,k} - T_{i,j,k})$$

$$+U_5A_5(T_{i+1,j,k} - T_{i,j,k}) + U_6A_6(T_{i-1,j,k} - T_{i,j,k})$$

$A_m$ is the area of each face and $U_m$ is defined as the overall heat transfer coefficient across each face m as shown in Fig. 2.2.

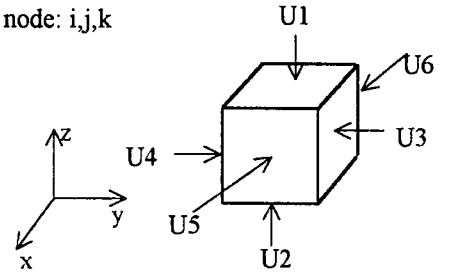


Figure 2.2 - Heat transfer coefficients on corresponding faces of a 3-D node

Overall heat transfer coefficients are used in this discretization to account for the heat conduction from one material to another as takes place in a printhead composite structure. For conduction in a uniform solid the overall heat transfer coefficient, U, would simply be $U = \frac{k}{L}$ where k is the thermal conductivity and L is the distance between the driving temperature differences. Fig. 2.3 shows an example of how this coefficient can be used in analysis for conduction from material A to material B each having unique lumped temperatures. Materials A and B have thermal conductivities $k_A$ and $k_B$ and thicknesses $L_A$ and $L_B$ respectively. The heat transfer coefficient for this geometry, neglecting contact resistance between the layers, is calculated as

$$U = \frac{1}{\frac{L_A}{2k_A} + \frac{L_B}{2k_B}}$$

The heat transfer from A to B is then given as:

$$Q = UArea(T_A - T_B)$$

where Area is the cross sectional area between the two materials.

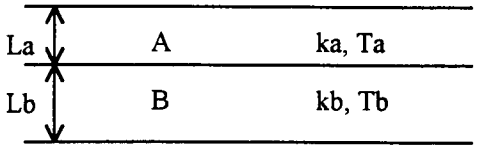


Figure 2.3 - Example of overall heat transfer coefficient calculation

Convection heat transfer can be handled similarly where U equals the convective heat transfer coefficient, h. So, mixed heat transfer from a solid to fluid with convective heat transfer coefficient, h, can be represented as:

$$Q = UA(T_A - T_B)$$

where $$U = \frac{1}{\frac{L}{2k} + \frac{1}{h}}.$$

The time derivative in equation (2.2) can now be discretized so that the solution for each node can be marched through time. Traditionally, this may be accomplished by a time marching scheme such as the simple explicit Euler method where the time derivative is approximated by differential increments $\left(\frac{\partial T}{\partial t} \rightarrow \frac{\Delta T}{\Delta t}\right)$ and both sides are multiplied by $\Delta t$ to solve for the temperature difference across one time step. Advanced variations of this scheme such as the Runge-Kutta and Adams-Bashforth methods can also be used for increased accuracy (Hoffman 1992). For this model, the Asymptotic Integration Algorithm (AIA) as described by Walker and Freed (1991) was used to solve the time derivative. The AIA method provides the advantage of high accuracy and stability for the small nodal spacings and large forcing term involved in solving equation (2.2) for the

printhead geometry. This method requires that both sides of equation (2.2) be multiplied by dt so that $T_{i,j,k}$ can be integrated across a time step. This result is then rearranged to get $T_{i,j,k}$ on one side of the equation as given in the final form, equation (2.3).

$$T_{i,j,k}^{n+1} = \frac{V_{i,j,k}}{W_{i,j,k}} - \left(\frac{V_{i,j,k}}{W_{i,j,k}} - T_{i,j,k}^{n}\right) e^{-W_{i,j,k}\Delta t} \tag{2.3}$$

where:

$$V_{i,j,k} = \frac{1}{(\rho c_p)_{i,j,k}}[Q'''_{i,j,k} + U_1(\Delta x \Delta y)T_{i,j,k+1} + U_2(\Delta x \Delta y)T_{i,j,k-1} + U_3(\Delta x \Delta z)T_{i,j+1,k}$$

$$+U_4(\Delta x \Delta z)T_{i,j-1,k} + U_5(\Delta z \Delta y)T_{i+1,j,k} + U_6(\Delta z \Delta y)T_{i-1,j,k}]$$

and

$$W_{i,j,k} = \frac{1}{(\rho c_p)_{i,j,k}}\left[\frac{U_1}{\Delta z} + \frac{U_2}{\Delta z} + \frac{U_3}{\Delta y} + \frac{U_4}{\Delta y} + \frac{U_5}{\Delta x} + \frac{U_6}{\Delta x}\right]$$

The superscript n indicates the time step while the i,j,k subscripts specify the current node in the x, y, and z directions, respectively. The $V_{i,j,k}$ coefficient is dependent on neighboring nodal temperatures and must be calculated for each time step. For temperature independent properties and boundary conditions, the $W_{i,j,k}$ coefficient stays constant throughout the simulation depending only on material properties and grid size.

Bubble Nucleation and Growth

The homogeneous vapor nucleation that occurs on a printhead's heater surface can be modeled by two general approaches. Either classical nucleation theory can be applied to predict the probability of a nucleation event occurring through time or a deterministic temperature can be specified as the point at which nucleation occurs. The latter approach is used here.

Different values have been used for this homogeneous nucleation temperature in the literature. Asai (1987) assumes a temperature of 270 °C, while Allen (1985) assumes nucleation at 330 °C. Runge (1993) developed an empirical relation to predict nucleation in a printhead thermal environment based on the temperature gradient in the ink:

$$K = \frac{T_{max}}{230 + 1.6 \times 10^{-7} \frac{\partial T}{\partial z}} \tag{2.4}$$

where $T_{max}$ is the maximum temperature of the ink and K must be equal to or greater than one for nucleation. For the model presented here, equation (2.4) was used to predict the occurrence of homogenous nucleation. Once the nucleation criterion is met through equation (2.4), it is assumed that vapor bubbles near the surface instantly combine to form a vapor film covering the heater surface and the bubble starts to grow.

The understanding of bubble growth under these high superheat, non-equilibrium conditions is limited and many simplifications are needed to model the process. In this work, three governing equations were used: a Newtonian equation of motion to represent the inertia of ink being moved by the bubble, conservation of energy across the bubble interface, and a state relation.

**Equation of Motion**

The equation of motion for the lumped liquid mass being pushed out of the nozzle by the high pressure bubble, assuming negligible viscous effects, is given by:

$$P_v - P_{atm} = (M\rho)\frac{d^2 Vol}{dt^2} \tag{2.5}$$

where Vol is the volume of the bubble, $P_v$ is the vapor pressure within the bubble, and M is the inertance factor. The ink is represented as water and is considered incompressible. This also assumes that the bubble only pushes ink out of the nozzle and backflow into the refill chambers during firing is ignored. This equation is physically the same as the

classical F=ma equation of motion. It represents the acceleration of a volume of fluid as a pressure difference is applied across its cross-sectional area. In equation (2.5), Mρ is the inertance of the fluid and is analogous to the mass in the F=ma equation, representing the element that opposes a change in volume current. This concept of inertance is used in acoustical engineering and is described by Olson (1942). Inertance is useful in this type of analysis when a driving pressure is being applied to a volume of fluid over a non-uniform cross-sectional area, which is the case of the ink fluid being pushed through the orifice of an inkjet printhead. The inertance factor, M, for a non-uniform cross-sectional area must be integrated along the length of fluid being accelerated and can be expressed as:

$$M = \int_0^L \frac{1}{\text{area}(x)} dx \tag{2.6}$$

For this model, equation (2.6) is evaluated from the bubble surface to the top of the drop slug that is being pushed out. The column of fluid that sits above the growing bubble is assumed to be pushed straight up through the nozzle, not entraining any fluid outside the model boundary (Fig. 2.1). Estimating fluid flow in this bulk manner for this application has precedence in Elger (1986) and Asai (1987).

**Energy Conservation**

Next an energy balance must be specified across the bubble interface since energy has to be transferred from the layer of superheated fluid above the bubble into the vapor for stable bubble growth (Hsu 1976). Equation (2.7) dictates the heat influx required for a given bubble growth rate, $\frac{\partial Vol}{\partial t}$.

$$A_{bubb} k_f \left(\frac{\partial T}{\partial z}\right) = h_{fg} \rho_v \frac{\partial Vol}{\partial t} \tag{2.7}$$

$A_{bubb}$ is the bubble surface area, $k_f$ is the thermal conductivity of the fluid, $\rho_v$ is the vapor density, and $\frac{\partial T}{\partial z}$ is the temperature gradient in the ink at the bubble interface. Equation (2.7) contains the assumption that the specific heat of the vapor is negligible so that all

energy conducted into the bubble contributes solely to phase change. Also, changes in vapor density are ignored. A similar conservation equation was used by Plesset (1954) and Asai (1987) in modeling bubble growth.

The gradient term in equation (2.7) and (2.8) requires knowledge of the fluid temperature above the bubble surface. Since, the temperature profile above the surface is dependent on the operating conditions of a specific run, a general scheme is needed to account for the amount of superheated liquid in the fluid at the nucleation point. To accomplish this, the temperature distribution in the first five fluid nodes against the heater surface is recorded at the time of nucleation. This temperature profile is then used in calculating the $\frac{\partial T}{\partial z}$ term at the bubble surface during the subsequent bubble growth calculations through a numerical differencing approximation: $\frac{T_{ink} - T_{bubble\ surface}}{\Delta z}$. $T_{ink}$ is the temperature of the first node recorded at nucleation. As the bubble grows, the recorded superheated temperature profile diffuses into the bulk of the fluid in the chamber. This is modeled as one-dimensional heat conduction, equation (2.8).

$$\frac{\partial T}{\partial t} = \alpha \frac{\partial^2 T}{\partial z^2} \tag{2.8}$$

Equation (2.8) is discretized and solved through a simple explicit Euler routine at each time step to find the temperature profile in the ink at the bubble surface.

$$T_k^{n+1} = T_k^n + \Delta t \alpha \frac{T_{k+1}^n - 2T_k^n + T_{k-1}^n}{\Delta z^2} \tag{2.9}$$

The domain that equation (2.9) solves is shown in Fig. 2.4.

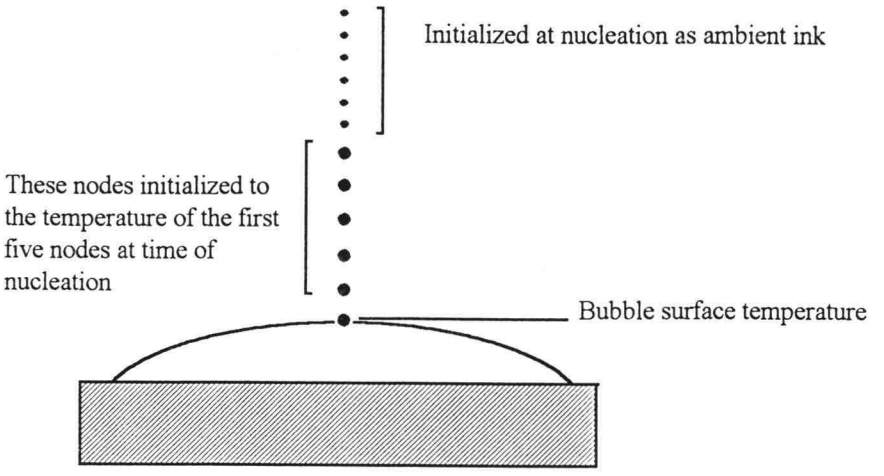


Figure 2.4 - Solution domain for heat conduction above bubble surface

This heat transfer calculation is done in conjunction with the rest of the bubble state calculations and is not associated with the calculations described in the Heat Transfer section earlier in this chapter. With the gradient term defined, equation (2.7) can be discretized and rearranged to find the decrease in vapor temperature at the bubble surface for the given growth rate (equation 2.10). This temperature drop represents the evaporative cooling that takes place as the bubble grows.

$$T_{\text{bubble surface}} = T_{\text{ink}} - \Delta z \frac{h_{fg}\rho_v \frac{dVol}{dt}}{A_{bubb} k_f} \qquad (2.10)$$

Equations (2.7) and (2.10) also require the surface area of the bubble. For this, some assumption about bubble shape must be made. It was assumed that the bubble stays attached to the entire heater surface and takes the shape of a spherical cap with the appropriate volume as depicted in Fig. 2.5. Since volume is solved through the governing equations and base length, b, is taken from the heater area, the height and surface area of the spherical cap can be found from geometric relations (Spiegel 1968).

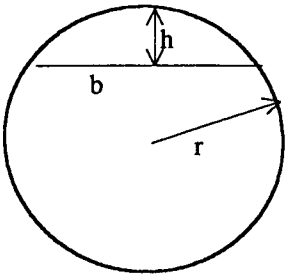


Figure 2.5 - Spherical cap geometry

Equation (2.11) gives the volume of the spherical cap as function of cap height (h) and base circle radius (r).

$$Vol = \tfrac{1}{3}\pi h^2(3r - h) \tag{2.11}$$

From the problem geometry, h, b, and r can be related through equation 2.12.

$$r^2 = (r - h)^2 + \left(\frac{b}{2}\right)^2 \tag{2.12}$$

Combining (2.11) and (2.12) results in a cubic equation with one unknown, h:

$$h^3 + \frac{3b^2}{4}h - \frac{6}{\pi}Vol = 0 \tag{2.13}$$

This particular cubic is classified as having two complex roots and one real root. Since only real roots are of interest, the solution for h becomes straightforward (Spiegel 1968). Once h is found, r can be calculated through equation (2.12) and surface area can be found through equation (2.14).

$$A_{bubb} = 2\pi rh \tag{2.14}$$

At birth, the bubble is very small so its corresponding base sphere is large. As the bubble grows, the cap gets larger and the corresponding sphere necessary to make that size cap gets smaller. This is illustrated in Fig. 2.6.

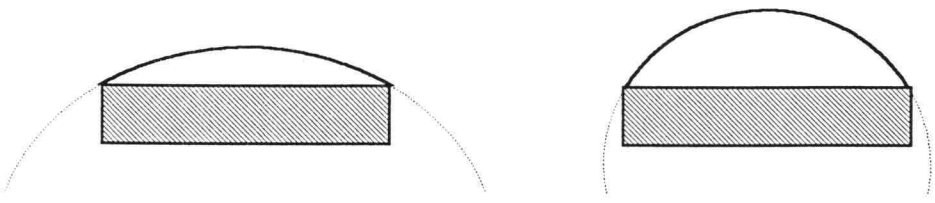

Figure 2.6 - Bubble shape modeled as spherical cap

**State Equation**

The vapor temperature solved through equation (2.10) is then used to solve for the vapor pressure. Traditionally, this pressure is modeled by using the equilibrium Clausius-Clapeyron relation, equation (2.15) (Moran 1992), as a state relation.

$$\frac{dP}{dT} = \frac{h_{fg}}{T(\upsilon_2 - \upsilon_1)} \tag{2.15}$$

Some modifications are necessary, though, so that it can be used to model the bubble growth process that takes place on a printhead's heater surface.

If both sides of equation (2.15) are multiplied by dT and then integrated across the properties of the phase change it takes the form:

$$P_v - P_{sat} = \frac{h_{fg}}{(\upsilon_{vap} - \upsilon_{liq})} \ln\left[\frac{T_{vapor}}{T_{sat}}\right] \tag{2.16}$$

The sat subscript indicates saturation conditions and $\upsilon$ is the specific volume. To account for the extra sensible energy accumulated in the superheated liquid before nucleation occurs, $h_{fg}$ must be replaced by an appropriate energy (E) that represents the transition between the two states in equation (2.16) as given by:

$$E = Cp_{liq}(T_{nucleation} - T_{sat}) + h_{fg} \tag{2.17}$$

Furthermore, the latent heat is replaced by an augmented latent heat which adjusts for the high temperature vaporization (Bromley 1950):

$$h_{fg}' = h_{fg} + 0.4Cp(T_{vap} - T_{sat}) \tag{2.18}$$

Combining equations 2.16-2.18 gives the governing state relation used in this model:

$$P_{vapor} - P_{sat} = \frac{h_{fg} + Cp_{liq}(T_{nucleation} - T_{sat})}{(\upsilon_{vap} - \upsilon_{liq})} \ln\left[\frac{T_{vapor}}{T_{sat}}\right] \tag{2.19}$$

This final form is used to find the pressure within the bubble from birth to death.

Ink Chamber Refill

In modeling the bubble growth, no backflow into the refill channel is considered and the ink evaporated into the bubble is assumed negligibly small ($\upsilon_{vap} >> \upsilon_{liq}$), so the ejected ink drop volume is assumed to be the same as the maximum bubble size. After bubble collapse, this volume of ink is assumed to refill the chamber as the final step in the firing process. Surface tension of the ink fluid at the nozzle is the primary mechanism for this refill and takes on the order of 100 $\mu$s to finish (Clark 1996). The refill channel connects to the ink chamber near the heater surface resulting in a flow of ink directly over

the surface, effectively cooling the surface with ambient temperature ink. It was found that this forced convection cooling effect in the refill process is necessary to model multi-firing simulations because of the residual heat in the thin films. This residual thermal energy left to conduct into stagnant ink would heat the ink enough to produce a secondary nucleation through the nucleation criterion. In reality, the ink is being mixed during this phase, not allowing severe temperature gradients to develop in the ink.

In this model, the refill process is greatly simplified. After a bubble has finished growing and is assumed to have collapsed, a finite refill time is represented in the model as conduction into a fixed temperature fluid for the specified refill time. During this time, the heat transfer from the surface layer to the ink fluid is given by:

$$Q = UA(T_{surface} - T_{fluid}) \tag{2.20}$$

where:

$$U = \frac{1}{\frac{L_{surface\ film}}{2k_{surface}} + \frac{L_{first\ fluid\ node}}{2k_{fluid}}}$$

The heat transferred into the fluid during each time step for this refill time is totaled and used to calculate a bulk temperature for the fluid in the ink chamber after the refill is finished (equation 2.21).

$$T_{bulk} = \frac{Q_{refill\ total}}{(C_p \rho Vol)_{fluid}} \tag{2.21}$$

Numerical Implementation

The program written to implement the mathematical model described here was written in the FORTRAN programming language. The program was written such that the nodal height ($\Delta z$) and material properties can vary from layer to layer to accommodate the

varying composite thicknesses and materials while nodal spacings in the lateral (x, y) directions are uniform throughout the grid.

For estimating the bulk fluid flow, nozzle shape was approximated as a linear cone as opposed to the curved shape of the nozzle as depicted in Fig. 2.7. The shape was represented in the code by specifying the top and bottom diameters.

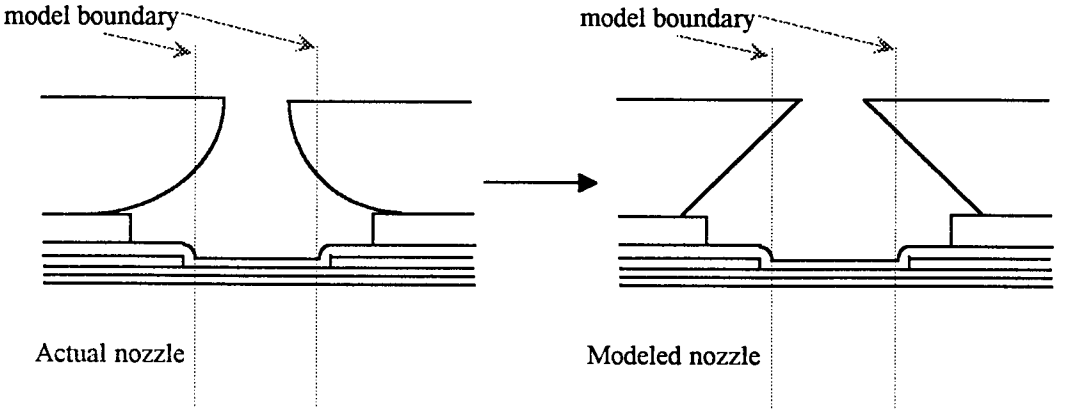


Figure 2.7 - Actual and modeled nozzle shape

The code received its input from two files. One file contained information on the thin film structure such as material identification and dimensions. This file also contained the electrical pulse height and width parameters. The second file was used to describe the grid used to discretize the fluid region of the domain including the top and bottom diameters of the nozzle.

The program's output involved several files. One file was used to record the temperature of the heater surface throughout the run. Bubble pressure and temperature were recorded in another file while bubble growth rate and volume were written to another file. Another output file was used to record any other information that was considered important for a particular run. Energy was another variable that was tracked throughout the run. This included the thermal energy in each thin film layer and the kinetic energy of the ink being pushed out by the bubble. This information was useful in determining efficiency of the printhead.

The calculation procedure is as follows. The code starts with the power pulse on, generating heat in the resistor layer corresponding to the pulse height in watts specified in the input file. During this time, heat transfer calculations are continuously solved throughout the structure and the fluid. At the beginning of each time step, the code compares the pulse width specified in the input file to the time that the pulse has been left on. If the pulse time exceeds the specified width, the pulse is turned off and the resistor stops generating heat but the conduction calculations still take place to solve for the heat diffusion.

The temperature distribution within the solution domain is solved at each time step through the solution of equation (2.3). Since equation (2.3) is dependent on its neighboring nodes, it must be iterated throughout the entire solution domain until a specified convergence criterion is met. The solution procedure for equation (2.3) is as follows:

1) coefficients V,U are evaluated at $T^{n}_{i,j,k}$
2) $T^{n+1}_{i,j,k}$ is predicted through equation (2.3)
3) coefficients V,U are re-evaluated at an average temperature:
$$T_{avg}=\frac{T^{n+1}+T^{n}}{2}$$
4) A new $T^{n+1}_{i,j,k}$ is predicted based on the average V,U coefficients
5) steps 3,4 are repeated until a convergence criterion is met
-end of heat transfer calculations for this time step

Bubble nucleation is checked for at the end of each time step. This is done by comparing the temperature of the fluid at the surface of the heater to equation (2.4). If this criterion has not been met, the heat transfer calculations continue as normal. If the criterion is met, then a vapor bubble of a pre-determined size is assumed to form across the heater surface and the initial vapor pressure is calculated from the nucleation temperature (equation 2.19). The temperature gradient in the fluid is also recorded at this time to be used in the subsequent bubble calculations. Once a bubble has been formed, bubble state calculations are performed at the end of each time step and the temperature field is only solved in the film structure.

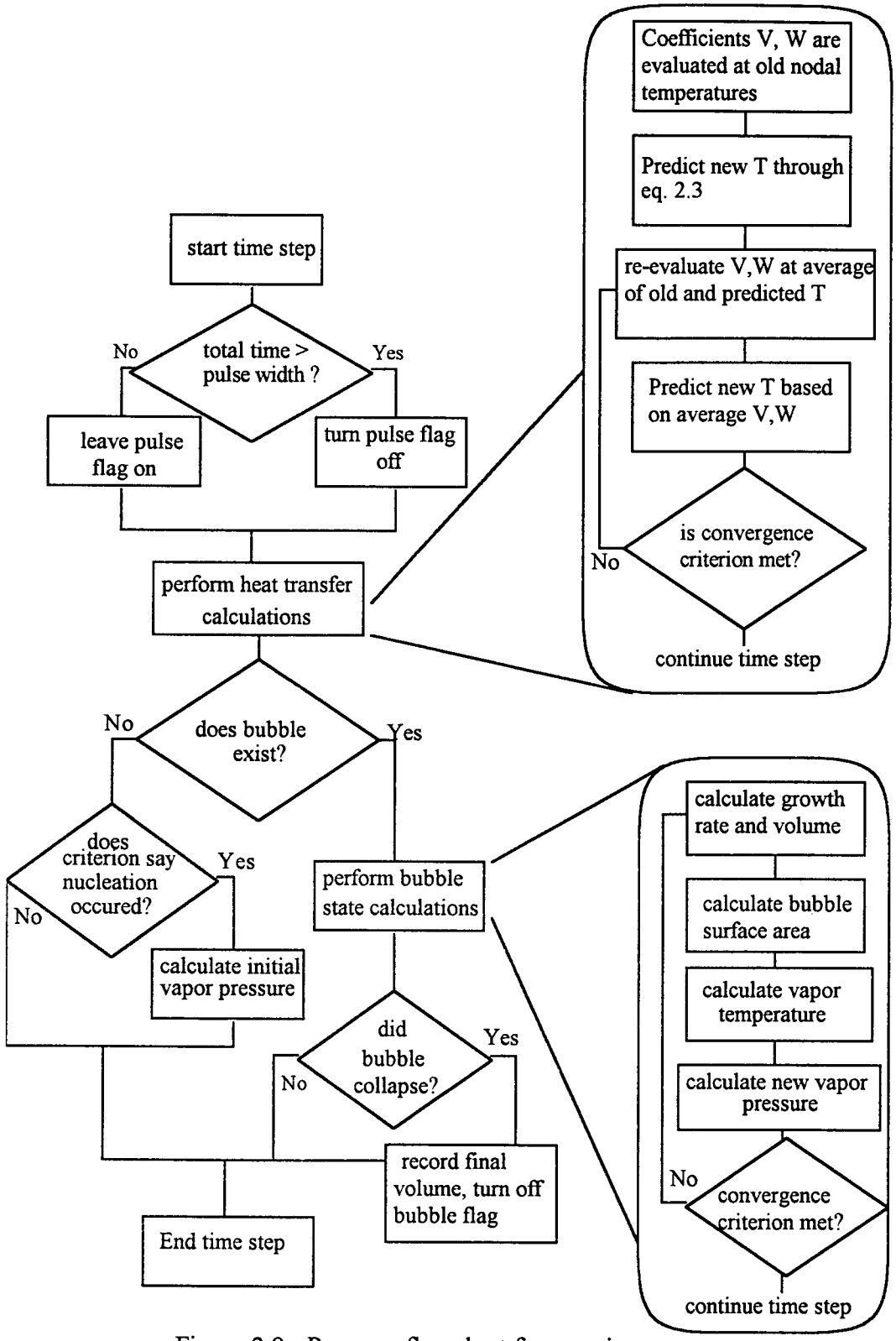


Figure 2.8 - Program flowchart for one time step

Equations (2.5), (2.10), and (2.19), in addition to information about bubble shape and ink temperature distribution, are all needed to describe the bubble growth process. Since growth rate is needed to find vapor temperature in equation (2.10) and thus vapor pressure in equation (2.19), which is used in finding growth rate, the motion and energy equations are coupled (Plesset 1954). For each time step when a bubble exists, these equations are iterated until the solution for bubble volume stops changing within a specified criterion to solve for a new bubble state (temperature, pressure, volume, growth rate). Eventually, the bubble cools to the point where it stops growing, reaching its maximum volume and begins to collapse. Since collapse mechanisms are not important in this study and we are only interested in how big the bubble grows, the model stops tracking bubble state at this point and assumes collapse.

Once the bubble has collapsed, ink chamber refill occurs. Refill is represented in the model as described in the Ink Chamber Refill section of this chapter for a designated time. During this time, the heat transfer from the heater surface is taken to be conduction into a constant temperature fluid. This is justified since fluid is rushing over the heater into the relatively large chamber. Once the refill time is finished, the solution domain for heat transfer is taken to be the film structure and ink chamber as before nucleation occurred, where the residual heat from the heater is conducted into the stagnant ink fluid. If multiple firings are being modeled, the diffusion of the leftover heat continues until the pulse cycle begins again. Fig. 2.8 presents a program flowchart which outlines this calculation procedure for one time step.

Boundary conditions in the model were handled through a "ghost node" technique. Ghost nodes are nodes defined outside the solution domain in order to impose the appropriate boundary conditions on the interior governing equations. Fig. 2.9 shows an example of ghost nodes for a simple two-dimensional domain.

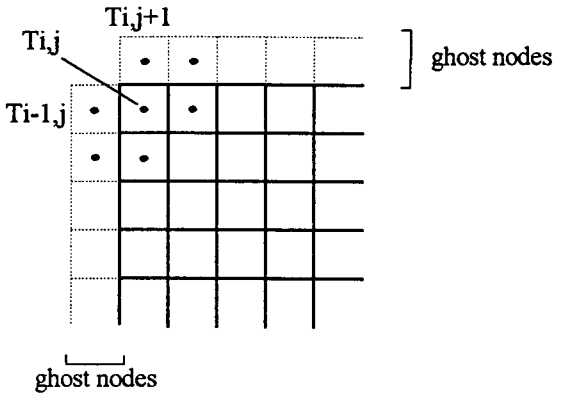


Figure 2.9 - Ghost node example

To implement a constant wall temperature boundary condition with this scheme, the average of the ghost node and its corresponding interior node would simply be set equal to the pre-defined wall temperature, $T_{wall}=\frac{T_{i-1,j}+T_{i,j}}{2}$. For a constant wall heat flux, the temperature for each ghost node would need to be updated each time step to maintain the prescribed heat flux. Equation (2.21) shows how the temperature at a ghost node could be defined for a constant wall heat flux.

$$q''_{prescribed} = k\frac{\partial T}{\partial x} \Rightarrow T_{i-1,j} = T_{i,j} + \Delta x\frac{q''_{prescribed}}{k} \qquad (2.21)$$

A convective boundary condition can be arranged similarly:

$$-k\frac{\partial T}{\partial x} = h(T_{amb} - T_{surface}) \Rightarrow T_{i-1,j} = \frac{\left(2 - \frac{h\Delta x}{k}\right)T_{i,j} + 2\frac{h\Delta x}{k}T_{amb}}{2 + \frac{h\Delta x}{k}} \qquad (2.22)$$

Equation (2.22) can also be used as a general boundary condition. As $h \rightarrow \infty$, equation (2.22) represents a constant wall temperature boundary condition. As $h \rightarrow 0$, equation (2.22) gives an insulated wall boundary condition.

The boundary condition at the top of the nozzle was considered adiabatic while the sides of the structure were held at a constant wall temperature. This top boundary condition was justified since heat does not have time to diffuse to the top of the nozzle

before a drop is ejected and refill occurs, thermally mixing the ink. The boundary condition imposed on the sides of the model can only be a rough approximation since in reality, heat will diffuse out the sides and gradually raise the temperature of the surrounding material. This wall boundary condition was varied from adiabatic to constant wall temperature while comparing its effect to experimental results. It was found that realistic conditions are best represented by constant wall temperature boundary conditions at the sides. At the bottom of the silicon substrate, the heat was assumed to convect into a large sink of water representing the refill ink.

When a bubble exists on the heater surface a boundary condition is imposed on the heater surface and the temperature is only solved for in the thin film structure. This is handled by imposing a convective boundary condition at the heater surface allowing the surface to convect into vapor while a bubble exists.

# CODE VALIDATION

The numerical model presented in Chapter 2 was subjected to a number of tests to determine its ability to approximate the governing equations that were modeled. Trial runs were also made to determine how many nodes were necessary in the lateral direction (x, y) in each horizontal thin film layer. Increased computational speed over existing models was an additional goal of this project; this was considered throughout the code validation phase of the project in order to optimize speed while maintaining accuracy.

## Theoretical Comparison

The first step in this validation process was to verify the accuracy of the Asymptotic Integration Algorithm (AIA) method described in Chapter 2 in modeling the heat transfer governing equation (equation 2.1). To do this, a simple case was used so that a known analytical solution could be used for comparison to the numerical solution. The problem of transient heat transfer in a three dimensional cube was chosen as a test case since it was similar to the heat transfer in the actual model. The exact solution to this simplified heat conduction problem was taken from Carslaw and Jaeger (1959) and is given by

$$T(x,y,z,t) = \frac{64}{\pi^3}\Sigma_{p=0}^{\infty}\Sigma_{m=0}^{\infty}\Sigma_{n=0}^{\infty}\frac{-1^{p+m+n}}{(2p+1)(2m+1)(2n+1)}\times \tag{3.1}$$

$$\cos\left[\frac{(2p+1)\pi x}{2a}\right]\cos\left[\frac{(2m+1)\pi y}{2b}\right]\cos\left[\frac{(2n+1)\pi z}{2c}\right]e^{\frac{\pi^2}{4}\left[\frac{(2p+1)^2}{a^2}+\frac{(2m+1)^2}{b^2}+\frac{(2n+1)^2}{c^2}\right]\alpha t}$$

where a, b, and c are the cube's dimensions. For simplification, all physical lengths and material properties of the three dimensional cube were set to one in the analytical and numerical solution. Also, the initial temperature of the block was set to one while the boundary conditions on all six walls were held at zero so that the temperature distribution in the solution domain varied between zero and one. The three dimensional temperature fields that were solved through the exact and numerical methods were compared at the mid-section of the cube at several different elapsed times. Fig. 3.1 presents numerical solutions at an elapsed time of 0.03 seconds for several different grid sizes with a fixed time step. Also shown is the exact solution truncated to six summation terms. For comparison, a numerical solution from a more common Alternating Direction Implicit, ADI, scheme (Douglas 1962) is included. These results show that the AIA numerical solution holds excellent accuracy even for a very coarse mesh. Also presented are the execution time for each numerical solution. The AIA method is at least two orders of magnitude faster than the ADI solution while holding better accuracy.

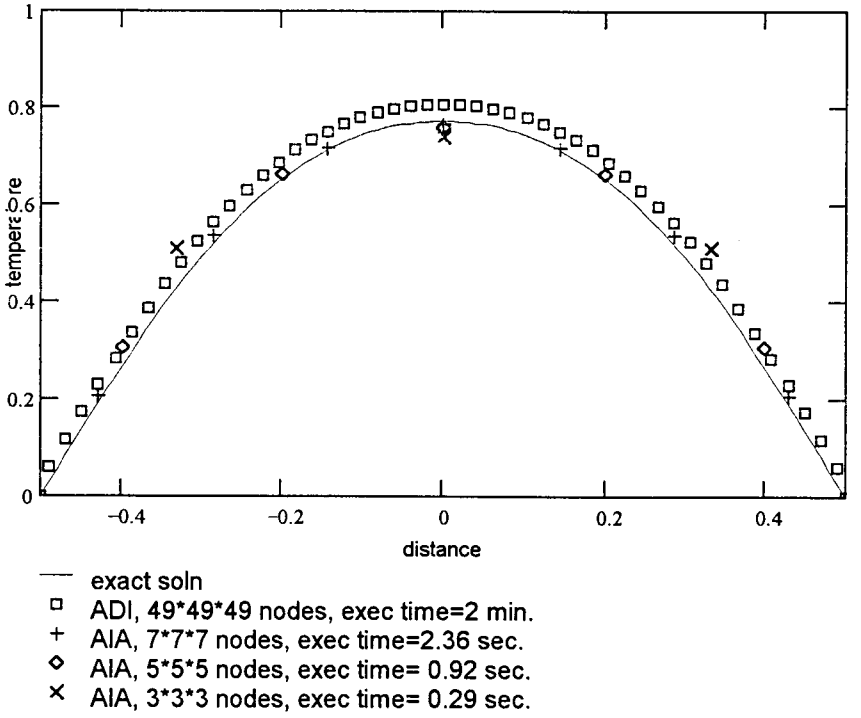


Figure 3.1 - Comparison of exact and numerical solutions for different grid sizes

A similar test was performed to study the effect of varying time step size on the AIA method. Fig. 3.2 shows the numerical solution for three different time steps with a constant grid size compared to the exact solution. This shows that accuracy for time steps of 0.001 and less is high for this geometry.

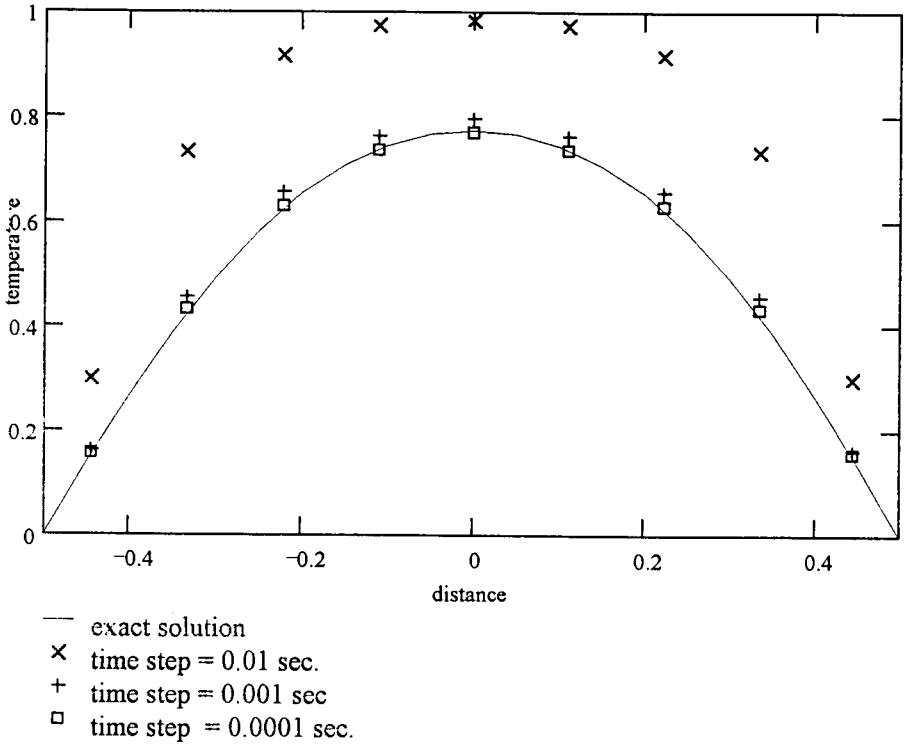


Figure 3.2 - Comparison of exact and numerical solutions for different time step values

Error Testing on Actual Geometry

Next, the numerical heat transfer calculations were tested on the actual geometry of the inkjet printhead. Tests performed in this step checked the effect of time step and node spacing variation on the total error of the solution. The error was estimated globally

by comparing the conserved quantity, energy, before and after the simulation. For zero error, the total energy in the domain, however distributed, had to equal the input energy plus initial energy plus any energy loss at the boundaries. These tests were kept simple by ignoring phase change in the liquid, considering only the heat transfer across the structure.

A typical thin film inkjet structure was used as a basis for the model geometry. Fig. 3.3 shows a two-dimensional slice of the inkjet composite. Dimensions and material properties for the structure are given in Fig. 3.4 (Clark, Knight 1996). Fig. 3.3 represents the material inside the step and does not include the aluminum layer. The total structure represented in the model is 42 μm square and 628.29 μm tall. The barrier material between the orifice plate and thin film stack is 26.5 μm thick while the orifice plate is 52.1 μm thick. The orifice has an inlet bore of 142.2 μm and an exit bore of 41 μm. All physical dimensions and properties of the model including pulse width and height are defined in the code's input files.

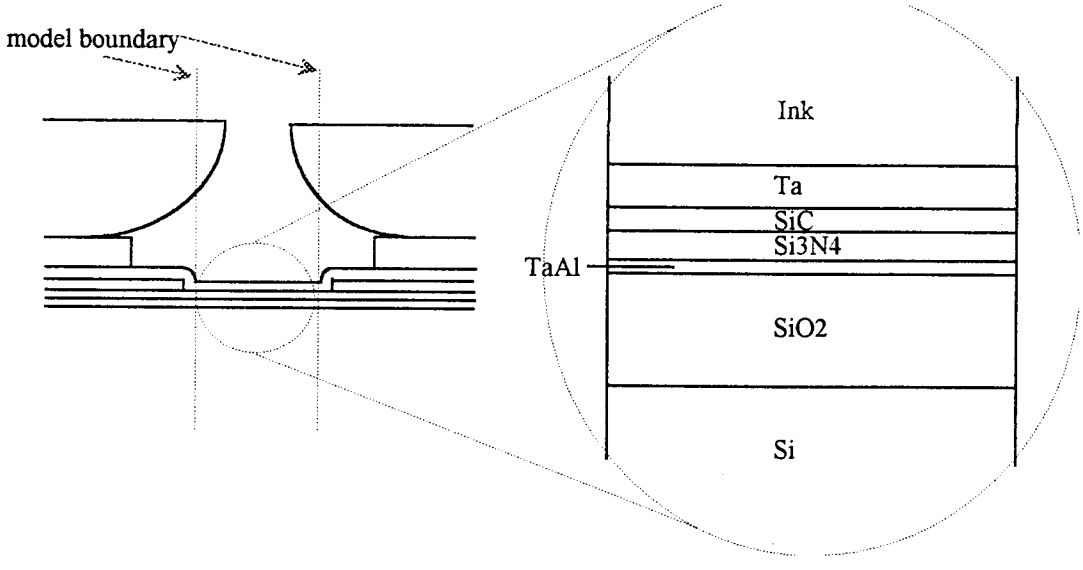


Figure 3.3 - Model Geometry

| Material | Heat Capacity ($J/m^3K$) | Conductivity (W/mK) | Thickness (μm) |
|---|---|---|---|
| Si | $165(10^4)$ | 140 | 625 |
| $SiO_2$ | $308(10^4)$ | 1.4 | 1.7 |
| TaAl | $236(10^4)$ | 144 | 0.09 |
| $Si_3N_4$ | $183(10^4)$ | 1.1 | 0.5 |
| SiC | $200(10^4)$ | 1.2 | 0.25 |
| Ta | $223(10^4)$ | 57 | 0.75 |

Figure 3.4-Material data from Knight, Clark

A uniform heat generation of 3 W was applied to the resistor layer for 3 μs resulting in a total energy of 9 μJ into the system. As discussed previously in Chapter 2, boundary conditions were insulated on the top and bottom layers while the side walls were maintained at a constant temperature of 20 C. The step size in the transverse direction varied with the respective film thicknesses with one node in the vertical direction per thin film layer. These tests showed that dividing the domain in the lateral directions has little effect on the solution. The temperature profile in these directions remains relatively flat, therefore resolution in these directions is not necessary. It was concluded from this that only one node is needed in the lateral direction resulting in one lumped node per thin film. However, the ability to obtain resolution in the lateral directions remains in the code to accommodate future studies. Fig. 3.5 presents the global error versus time step.

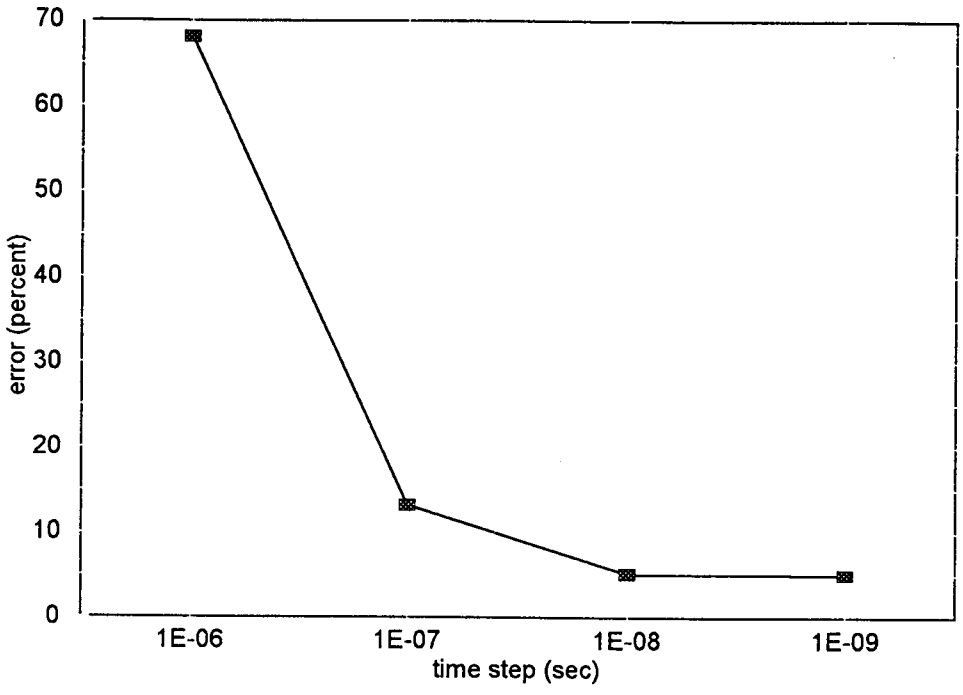


Figure 3.5 - Global numerical error versus time step

As expected in any numerical approximation, the error decreases with decreasing time step size. This result shows that a time step no larger than 1e-8 gives only 5% error in the energy conservation calculations.

The theoretical testing presented here has shown that the numerical method used for solving the heat transfer equations is very accurate and that the temperature distribution in the actual geometry can be solved with acceptable accuracy. The time and spatial steps used in the numerical solution have also been optimized for accuracy and computational speed.

# RESULTS

The model is able to generate several types of information that are useful in describing the firing process of a printhead. These results fall into two general categories: the thermal characteristics of the thin film structure, and the bubble/ink drop properties. A thermal efficiency was also defined for the printhead in order to describe the pen's performance in a global manner. This thermal efficiency was used to perform a system wide parametric study. This was done to see the effect of varying key system parameters on a printhead's thermal efficiency.

Finally, the model was used to predict ink drop mass and velocity as a function of pulse energy. These data are important in determining how the pen responds to different operating conditions. These predictions can be used in narrowing design options and reducing the number of prototypes built.

## Thermal Characteristics of the Structure

Solving the discretized energy equation (eq. 2.3) at discrete points across the solution domain is necessary to track the firing of a printhead. Therefore, information on temperature and energy distributions are easily obtained for any point in time. Fig. 4.1 shows the heater surface temperature for three consecutive pulses, while Fig. 4.2 magnifies the heater surface temperature trend for one pulse.

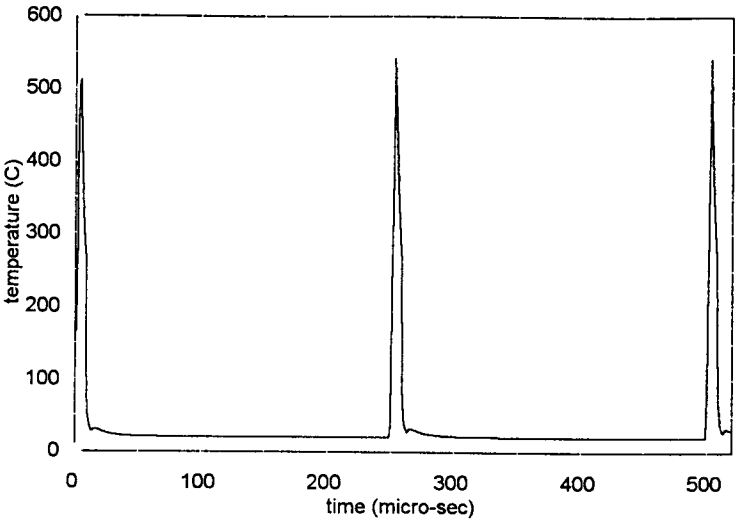


Figure 4.1 - Heater surface temperature for three pulses

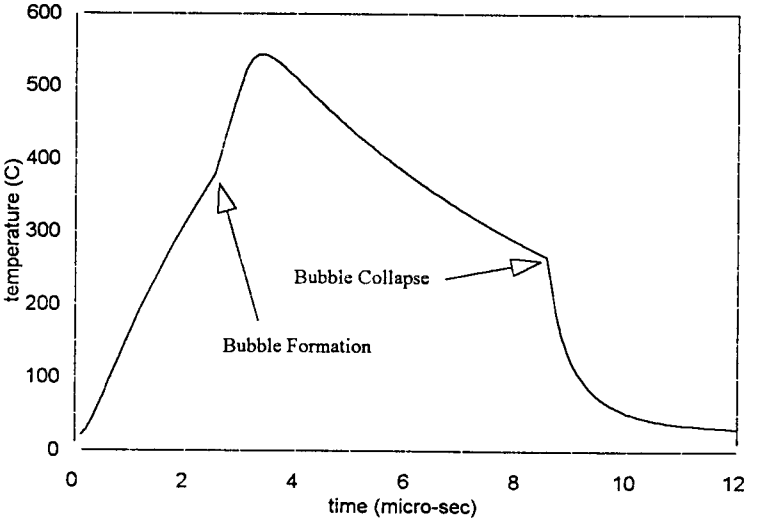


Figure 4.2 - High resolution heater surface temperature for one pulse

Two important events can be picked out of the temperature trend shown in Fig. 4.2. At around 2.5 μs, a nucleation event occurs in the fluid and a bubble starts to grow on the heater surface. This change from liquid to vapor results in a decrease of the thermal conductivity of the material directly above the solid surface. This is shown by the distinct increase in surface temperature versus time in Fig. 4.2. The inverse trend is seen when the bubble collapses at around 8.5 μs. This collapse results in an increase in the thermal conductivity next to the surface causing higher heat transfer rates. Also, refill occurs at this point in time, resulting in ambient temperature ink flowing over the surface. This enhanced heat transfer at the surface produces the drastic temperature drop shown in Fig. 4.2. The maximum temperature in Fig. 4.2 corresponds with the pulse being turned off.

Another important piece of information that can be obtained through the solution of the energy equation is the temperature profile in the thin film stack in the transverse direction. Fig. 4.3 shows such a temperature profile at the point of nucleation (~2.5 μs).

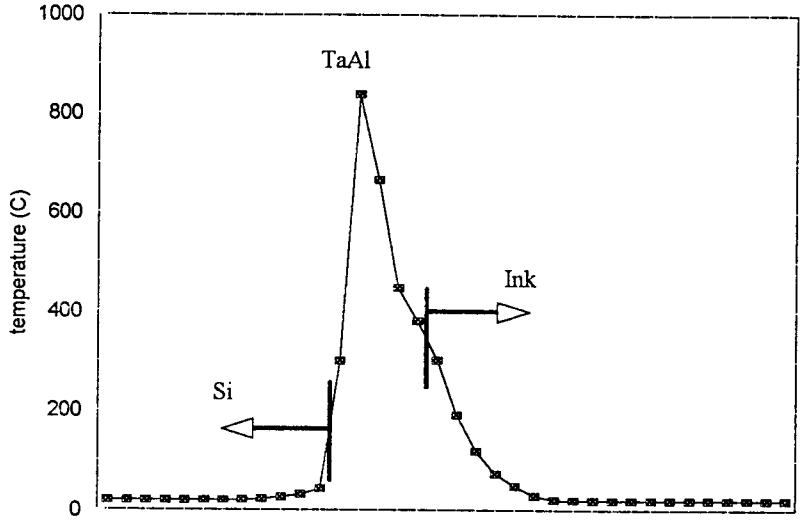


Figure 4.3 - Temperature profile in the thin film structure at the time of nucleation

Since each thin film has its own unique temperature dependent thermal and mechanical properties (e.g. coefficient of thermal expansion), the temperature gradient shown in Fig.

4.3 produces large mechanical stresses (Aden 1994). Therefore, this information is important in predicting the stress distribution in the structure.

Ideally, all the energy from the pulse would be deposited in the ink and not spread over the entire structure. In reality, the energy is diffused over the entire thin film structure. Since each film has its own unique thermal properties, the energy distribution is not uniform. The model is capable of predicting this thermal energy distribution in the printhead structure. Fig. 4.4 shows the distribution of energy in the different thin film layers given in table 3.1. This energy distribution is at the point of nucleation (~2.5 μs) with a 3 W, 3 μs applied pulse.

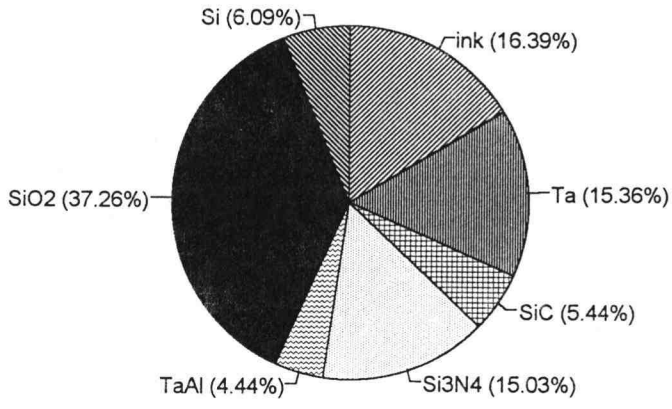


Figure 4.4 - Printhead energy distribution at time of nucleation

This shows that only 16.4% of the applied energy has entered the ink at this time, while most of the energy is absorbed by the $SiO_2$ layer under the resistor. At this short time duration, the energy loss out the sides of the model was negligible.

Bubble Characteristics

Information on vapor bubble state can also be gathered from the model. Fig. 4.5 shows the bubble growth process by tracking the bubble volume and volumetric growth rate from birth to death for a 3 W, 3 μs pulse.

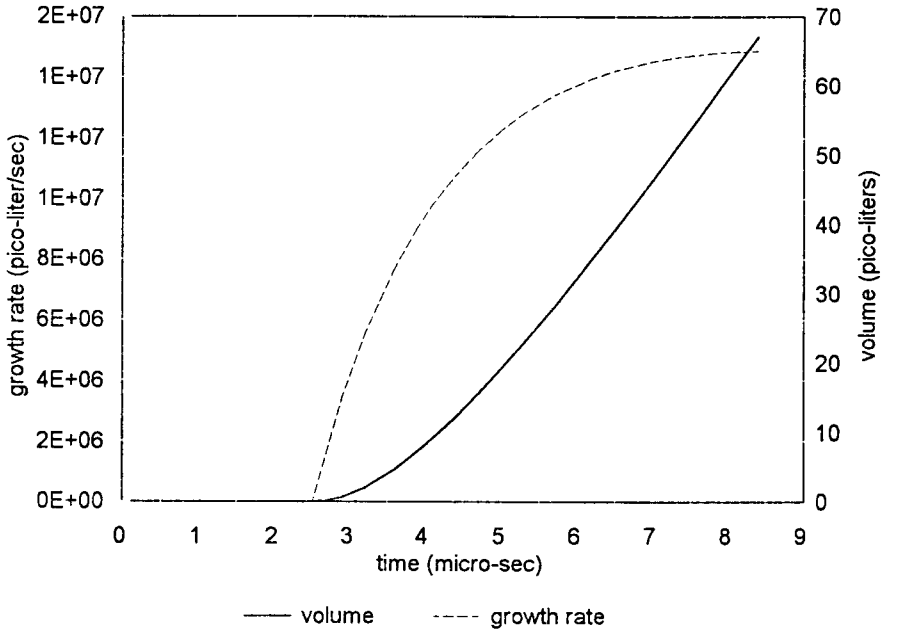


Figure 4.5 - The bubble growth process

Fig. 4.5 shows how the growth rate slows to maximum as the bubble grows and cools. This maximum is associated with the vapor state returning to saturation conditions. At this point the bubble is assumed to condense and collapse.

The vapor pressure throughout the life of the bubble can also be an important result. This information can be used as input to more sophisticated computational fluid

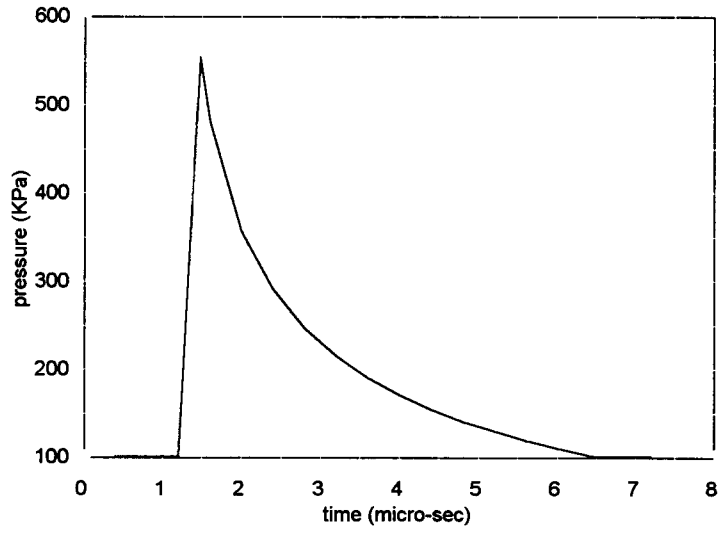


Figure 4.6 - Pressure history for the life of the vapor bubble

The initial spike seen in Fig. 4.6 is the vapor pressure at nucleation. This high pressure is a result of the high nucleation temperature associated with inkjet operation. As the vapor temperature drops, due to evaporative cooling, the vapor pressure decreases as well until the bubble collapses at 100 KPa.

## Parametric Studies

A parametric study was conducted to determine the effect of varying system parameters on pen performance. The pen performance was measured through a dimensionless figure of merit representing the thermal efficiency of the printhead. This efficiency was defined as the kinetic energy of the ink drop divided by the thermal energy supplied to the system through the resistor in the thin film structure (equation 4.1).

$$\eta_{th} = \frac{\frac{1}{2}\text{mass}_{drop}\text{Vel}^2}{\text{energy}_{pulse}} \tag{4.1}$$

As stated earlier, the drop mass was taken as the maximum volume of the bubble times the density of the ink fluid. The drop velocity was taken simply as the volumetric rate of the ink divided by the nozzle exit area.

The change in this efficiency was observed as each parameter or combination of parameters was varied. Seven parameters (or statistical *factors*) were chosen to vary for this study: the thickness of each layer built on top of the Si substrate, the surface area of the heater, and the pulse height while keeping pulse width constant. In addition to looking at the effect of each factor on the efficiency, it was desired to observe any interaction between the factor variations. For example, how does changing the thickness of the $SiO_2$ layer effect the relationship between surface area and efficiency? To describe every interaction of these variables, a full factorial experimental design would be needed. The number of runs necessary for a traditional two level factorial design is given by equation (4.2).

$$\text{runs} = 2^{\text{factors}} \tag{4.2}$$

For this study, equation (4.2) dictates 128 runs to completely describe the system variable's interactions for only two levels of variation. However, there are a number of partial factorial designs that have been proposed to reduce this number of runs while still adequately describing the system. One such partial factorial is the Box-Behnken three level design (Box, 1960). This design allows three levels of variation per factor while reducing the numbers of runs necessary relative to a full factorial design. The three levels of variation are useful because it lends itself to picking up non-linear behavior while two levels will only show linear responses. Only 57 runs are necessary with the Box-Behnken design for a 7 factor, 3 level system while a full factorial would require 2187 runs. Levels for each factor were chosen by varying each parameter by $\pm 10\%$ as shown in Fig. 4.7.

| Factor | low level | mean level | high level |
|---|---|---|---|
| SiO2 Thickness (um) | 1.53 | 1.7 | 1.87 |
| TaAl Thickness (um) | 0.081 | 0.09 | 0.099 |
| Si3N4 Thickness (um) | 0.45 | 0.5 | 0.55 |
| SiC Thickness (um) | 0.225 | 0.25 | 0.275 |
| Ta Thickness (um) | 0.675 | 0.75 | 0.825 |
| Heater Surface Area (um square) | 37.8 | 42 | 46.2 |
| Pulse Height (watts) | 2.7 | 3 | 3.3 |

Figure 4.7 - Parameter variations

MiniTab Statistical Software, a commercial package, was used to construct the Box-Behnken experimental design and to perform the required response analysis once the 57 runs were made with the model.

Two important pieces of information fall out of the statistical analysis: the effect of the individual factor variations on efficiency and the interaction effects between factors. Fig. 4.8 shows the main effects plot presenting each parameter's individual effect on efficiency. The main effects plot shows that the thicknesses of the thin films had little effect on pen performance. This result indicates that changes in the thermal properties of the thin films have little effect on pen performance. However, heater surface area and pulse height did have a noticeable effect on efficiency. The heater surface area effect is easily predicted through the bubble geometry assumptions. Since the bubble is assumed to cover the entire heater area, the bubble's surface area will increase with heater area, resulting in more heat transfer from the superheated ink to the bubble. The pulse height's inverse effect is due to the ink nucleating sooner with higher pulse height. This results in less time for the superheated thermal layer to grow in the ink. The thinner superheated ink layer provides less energy to the bubble, restricting growth.

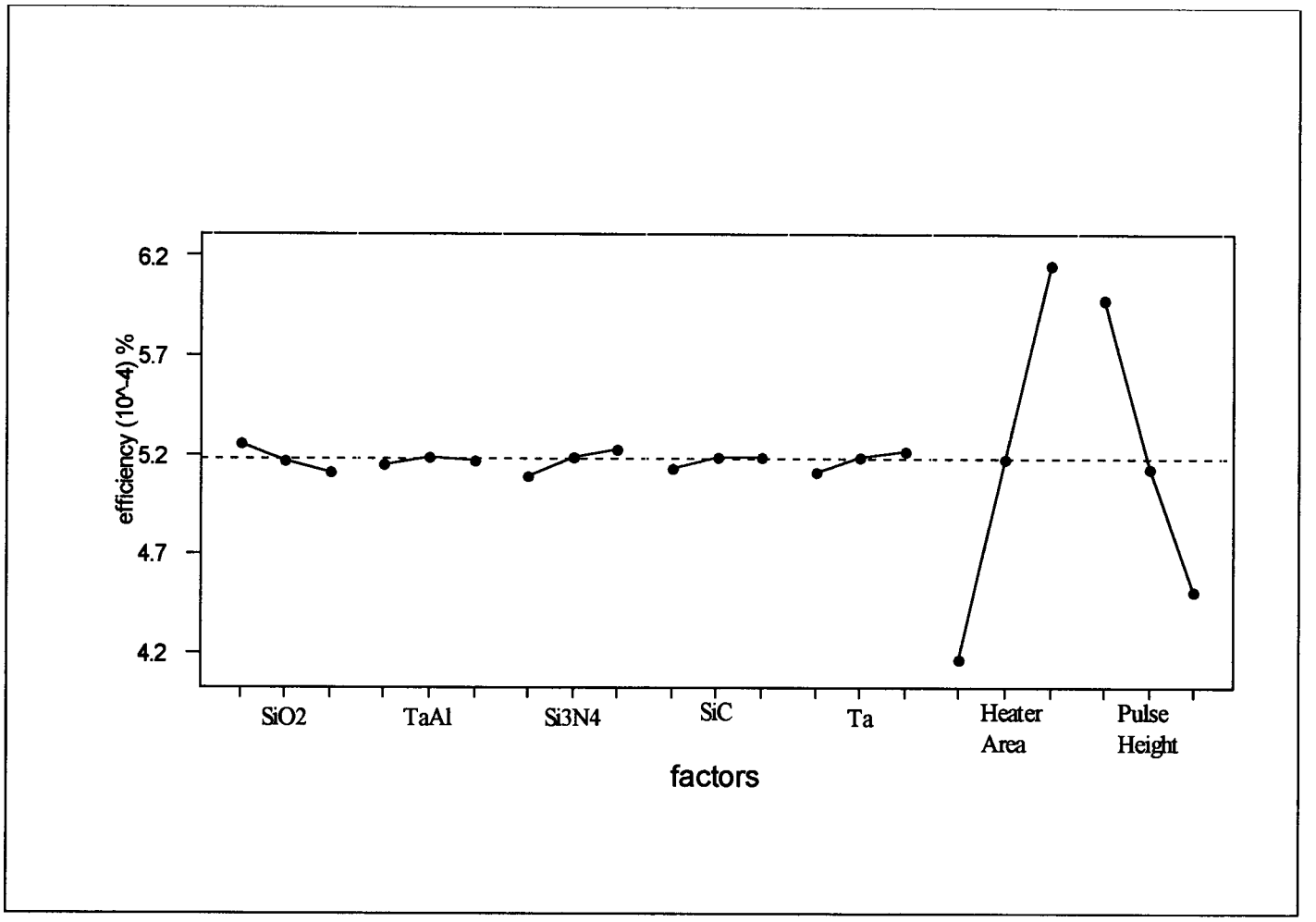


Figure 4.8 - Main effects plot. Individual parameter effects on efficiency

Fig. 4.9 presents the parameter interaction plots. This collection of graphs shows the interaction effects between factors. Each individual plot represents the interaction between the two factors in the plot's corresponding row and column. The vertical axis of each graph is in units of the response variable, efficiency. The horizontal axis shows the levels of the factor in the plot's column. The different lines represent the different settings of the factor in the plot's row. For example, the plot in the lower right corner of Fig. 4.9 shows how efficiency changes with pulse height for three different surface areas. This indicates how the influence of the pulse height on efficiency depends on the settings of the surface area in the corresponding row. A significant interaction between two factors would show up in one of the plots as lines with sharply differing slopes. A collection of lines on a given plot that are fairly parallel indicate that those interactions are not significant. As is seen in Fig. 4.9, the lines in the individual plots are fairly parallel meaning that the interaction between the printhead's system parameters is insignificant.

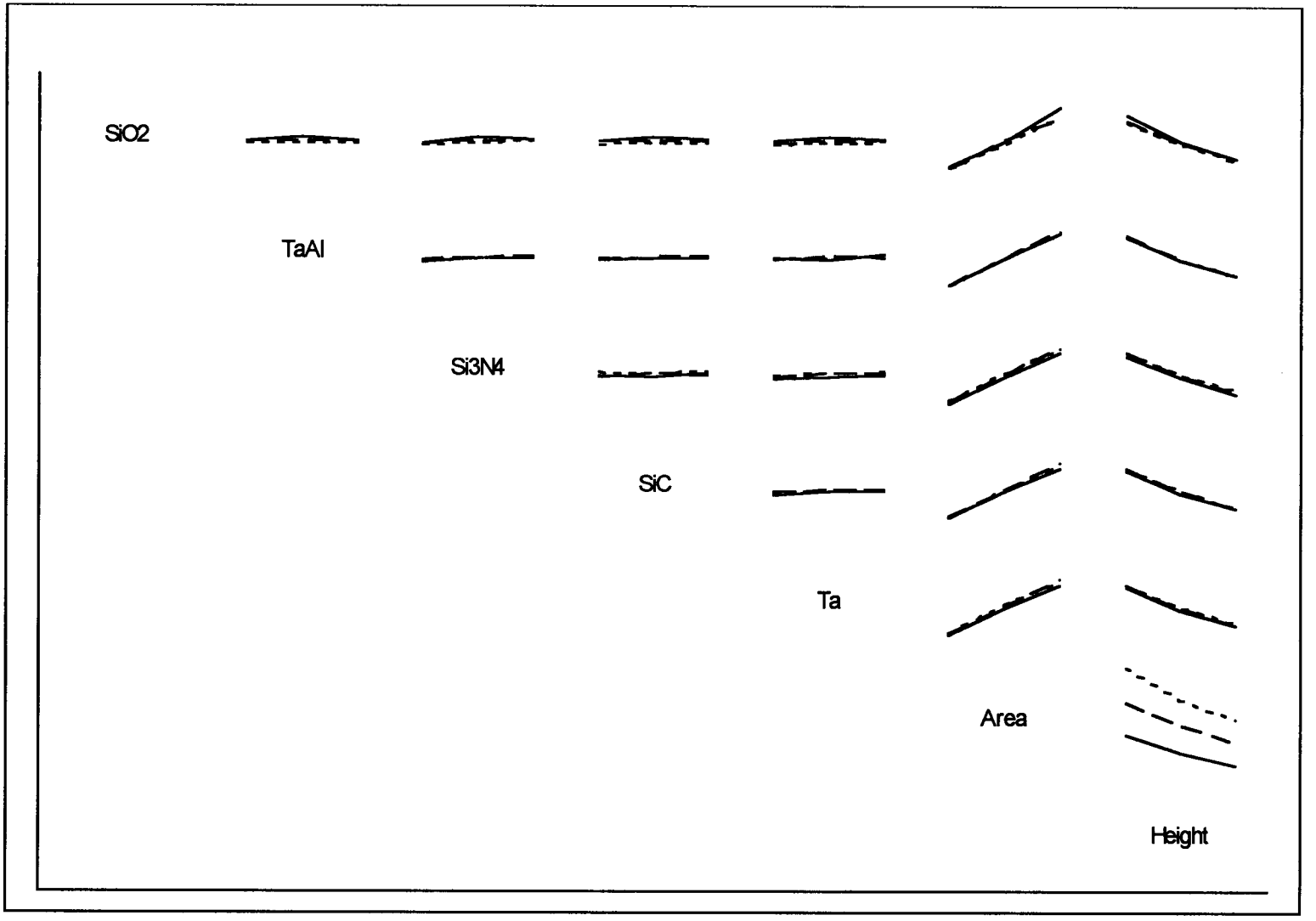


Figure 4.9 - Parameter interaction plot

Predicting Turn-On Curves

The model was used to predict ink drop mass and velocity as a function of pulse energy. This type of data is important in determining how the pen responds to different operating conditions. These predictions can be used in narrowing design options and reducing the number of prototypes built. These results were also used as a validation tool for the model since it enables the entire printhead firing process to be compared to existing experimental data provided by Hewlett Packard (Clark, 1996). This phase of validation not only shows if the equations are being solved correctly but also tests the assumptions and simplifications which have been made on the physical system. The data set available for comparison is that of individual ink drop mass as a function of total energy supplied to the thin film resistor in the printhead. These data show how much energy is necessary to produce an ink drop or "turn on" the printhead. Because of the information they present, these plots are typically called turn-on curves. A typical turn-on curve is shown in Fig. 4.10.

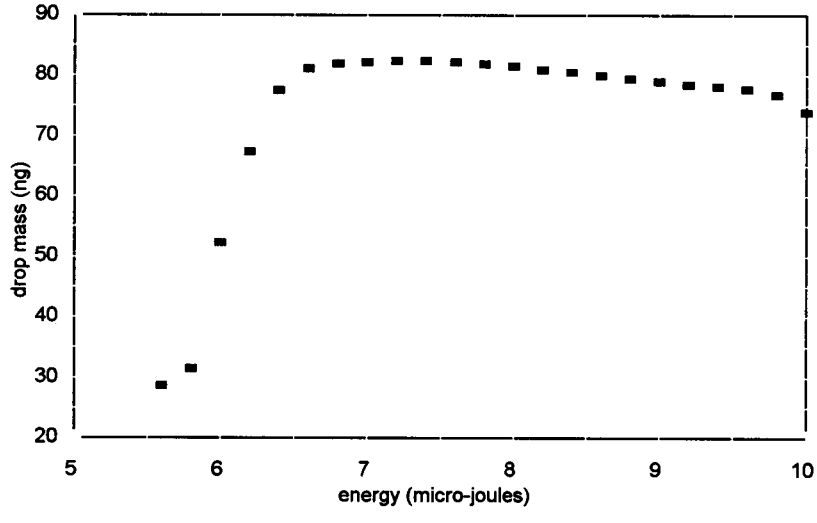


Figure 4.10 - Typical turn-on curve for a printhead

The data shown are averages of five different pen tests to account for pen to pen variation. The energy was changed by maintaining the pulse width at 2.4 μs while varying the pulse height in watts to achieve the desired total energy.

This plot shows a range of input energies to the right of the curve's knee (7.0-9.0 μJ) where the drop mass only varies by 6%. This is the desired range of operation since drop mass is easily predicted while maintaining a safety factor. Operating with an energy less than 6.5 μJ would produce drop masses that are less tolerant of input energy deviations. This range of the curve (5.5-6.5 μJ) would experience a lower heat flux and is probably influenced more by low temperature nucleation mechanisms (heterogeneous boiling) than homogeneous nucleation. These low temperature mechanisms would produce low vapor pressures reducing the drop mass and repeatability of the firings. Since the model described here only represents homogeneous nucleation as given by the temperature "switch" presented in equation (2.4), these low temperature effects can not be expected to show up in this model. Multiple cases were run with the model, maintaining pulse width at 2.4 μs and varying pulse heights from 5.0 to 10.0 watts in 0.2 watt increments. Fig. 4.11 plots these results along with the empirical results shown in Fig. 4.10.

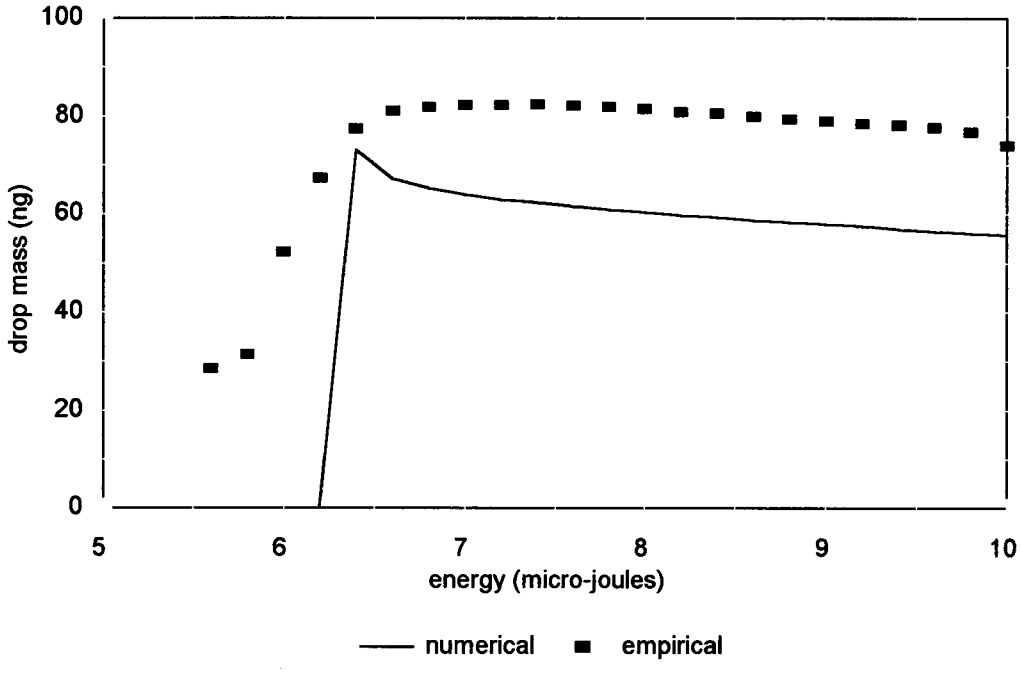


Figure 4.11 - Numerical and experimental turn-on curves

As expected, the numerical model does not predict the low energy (low nucleation temperature) drop masses. However, the model shows high temperature nucleation starting around 6.4 μJ, very close to the experimental curve's "knee". The drop masses predicted by the model stay within 20 ng of the values given by experiment. The most important trend is the model's ability to predict the decrease in drop mass as energy increases. This slope is matched very closely by the empirical results.

Fig. 4.12 presents drop velocities in a turn-on curve similar to Fig. 4.11. This shows that drop velocities are also closely approximated by the model in the high energy range.

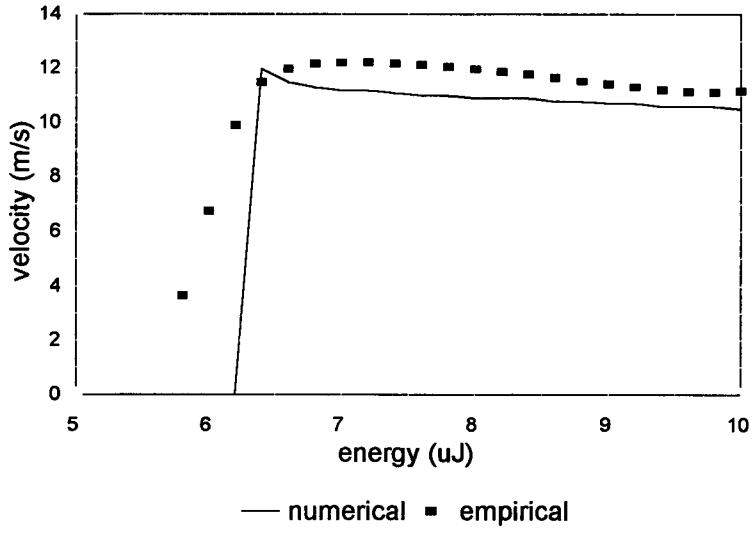


Figure 4.12 - Drop velocities versus input energy

The power pulse can also be varied in other ways to achieve a different response from the pen. This time the power pulse was split into two equal 1.2 μs parts with a variable delay between the two halves. As before, the total energy was controlled by changing the height of the pulses. Splitting the pulse in this way effectively preheats the ink, allowing a deeper thermal boundary layer to develop in the ink before nucleation. In the limit of no delay time between the two halves, the results would match Fig. 4.11. With increasing delay times, time to nucleation would be expected to increase until no nucleation occurred. But, if the pulse height is very large in conjunction with a large delay time, nucleation could be expected with the delay time taking the place of the period between the pulses. Cases were run with the model to see the effect of varying the delay time between two half pulses of equal height and duration. The total energy was varied between 5 and 10 μJ by changing the pulse heights. The experimental drop masses and the numerical results are shown in Figs. 4.13 and 4.14, respectively.

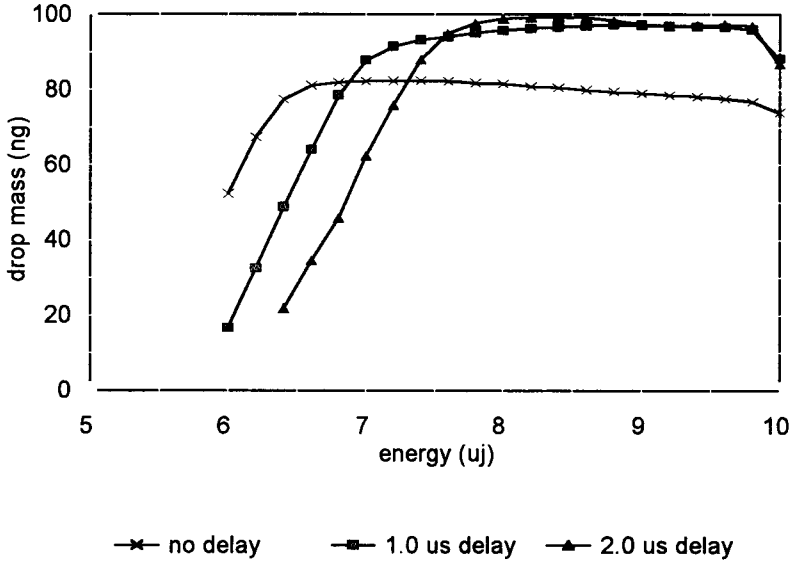


Figure 4.13 - Experimental drop masses for two pulse delay times

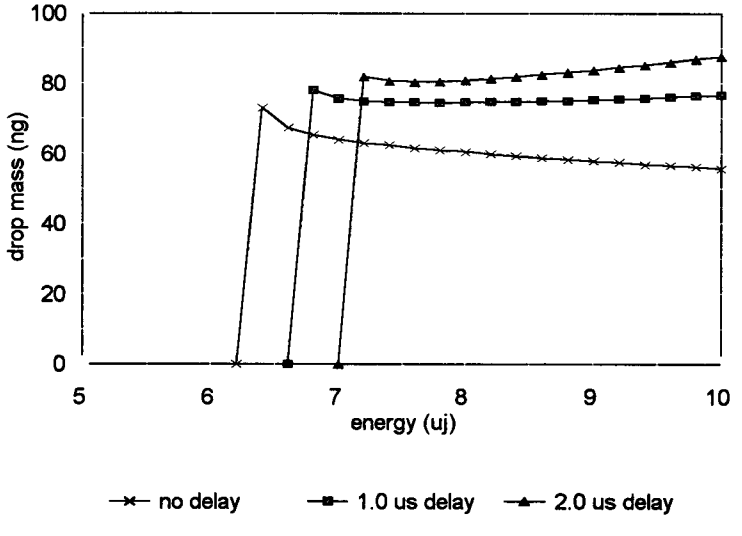


Figure 4.14 - Numerical drop masses for two delay times

As expected, the amount of energy necessary for nucleation increases with delay time. Also, drop masses increase with delay time probably due to the deeper layer of superheated ink feeding the bubble. The numerical results also show these trends of delayed nucleation and higher drop mass.

The comparison to experimental results presented here has shown the model's strengths and weaknesses. It was shown that the model is good at predicting the general trends shown by an actual inkjet as energy and pulse delay times are varied. However, it is important to note that the model does have many simplifications, resulting in the error shown in Figs. 4.11-4.14. Some of the important simplifications include neglecting low temperature nucleation mechanisms, neglecting viscous effects, and the limited domain being modeled (Fig. 3.3). Other more complicated processes being neglected include the effects of the drop separating from the bulk fluid and the three dimensional nature of the ink flow as the bubble grows.

# CONCLUSION

For this study, a numerical model has been built to simulate the firing process of a single thermal inkjet nozzle. The model includes the heat generation and diffusion within the thin film structure, the phase change and vapor bubble growth on the heater surface, and the subsequent ink drop ejection. The motivation for such a model comes from the desire to predict pen performance based on a full set of system parameters. The goals of the research were accomplished in three main steps: gaining an understanding of the physical processes and building of the numerical model, validating the model, and producing results used to describe the behavior of the firing process.

The heat transfer within the thin film structure was modeled by numerically approximating the conservation of energy equation through the asymptotical integration algorithm, as described in Chapter 2. The vapor nucleation was modeled through an empirical criterion based on the temperature gradient in the ink. Once a bubble was assumed to form, the bubble growth process was modeled through three governing equations (momentum, energy, state) that were solved simultaneously for each time step.

The model was validated with both theoretical and experimental data. The theoretical comparisons were made to test the accuracy of the numerical scheme used to model the heat transfer governing equation. This comparison showed that the numerical method used in this model is very good at approximating the analytical solution and is considerably faster, computationally, than other methods used for this application. The effect of time and spatial step sizes were also tested on the actual nozzle geometry to assure acceptable accuracy could be met. Comparison of experimental data to the model's results was used to determine how closely the actual physical processes were being modeled. This showed that the trends produced by an actual inkjet printhead were being simulated by the model for the given tests.

The model produced in this study is capable of producing many kinds of results that are useful in predicting different aspects of inkjet pen behavior. One of the more

important results is the model's ability to predict ink drop mass and velocity as a function of input energy. This prediction is useful in narrowing design options and limiting the number of physical prototypes built. Other significant data which can be produced by this model include temperature and energy profiles throughout the structure at any point in time. Bubble pressure and temperature history can be tracked through the life of a bubble as well as ink drop volume and speed. As shown in the parametric study, variables such as system efficiency can also be calculated.

Finally, the validated model was used to perform some basic parametric studies on the printhead's variable design parameters. A Box-Behnkin experimental design was used to determine the influence of parameter variation on thermal efficiency. This approach also made it possible to look at the interdependencies of the parameters. The study showed that changes in the thin film thicknesses (changing the characteristic diffusion time) do not strongly influence the system's efficiency. However, the heater surface area and the pulse height do have a strong influence on pen performance.

During the course of this research, several issues arose that could not be addressed within the scope of this project. The most important group of issues have to do with the phase change process. As mentioned earlier in this thesis, only high temperature nucleation was considered as a phase change mechanism. For high heat fluxes, the model agrees with experimental results. For low heat fluxes, however, when low temperature mechanisms may be dominant, a better nucleation prediction scheme is needed. An implementation of the stochastic, classical nucleation theory as used by Asai (1987) could improve this prediction since it incorporates both heterogeneous and homogeneous processes. Also, in this model, the bubble was assumed to instantly take the form of a thin vapor film across the heater surface at nucleation. In reality, discrete vapor pockets may form at different places on the surface at different points in time. If this process could be modeled, this instantaneous vapor film assumption could be tested and the effect of bubble quality on ink drop volume could be studied. The effect of a single vapor bubble forming on a corner of the heater and growing could also be investigated.

In addition, many refinements could be added to the numerical model built in this research. One obvious improvement would be to increase the physical range of the

computational domain to solve for more of the structure including the step formed by the aluminum conductor. Thermal properties are another area of interest that could be investigated. Specifically, incorporating the effects of the thin film's anisotropic thermal properties would make it possible to more accurately represent the heat transfer in the structure. Temperature dependent properties could also be used to this same end.

Finally, more detail could be added to the solution of the fluid flow produced by the bubble growth. This could include adding viscous effects, surface tension, and consideration of the backflow of fluid into the refill channel. More complexity could be added by coupling the full solution of the Navier-Stokes equations with the current thermal/phase change model to describe the drop ejection in detail.

The model in its current form, however, adequetely captures the trends in pen behavior as a function of several system parameters. This ability makes the model a useful tool in the early stages of printhead design.

# BIBLIOGRAPHY


Aden S, et al. The Third-Generation HP Thermal Inkjet Printhead. Hewlett Packard Journal. February 1994. pp. 41-45.

Allen R, Meyer JD, Knight, WR. Thermodynamics and Hydrodynamics of Thermal Inkjets. Hewlett Packard Journal, May 1985, pp 21-27.

Asai A, Hara T, Endo I. One-Dimensinal Model of Bubble Growth and Liquid Flow in Bubble Jet Printers. Japanese Journal of Applied Physics, Vol. 26, No.10, October 1987, pp. 1794-1801.

Asai A. Application of the Nucleation Theory to the Design of Bubble Jet Printers. Japanese Journal of Applied Physics, Vol. 28, No.5, May 1989, pp. 909-915.

Asai A. Bubble Dynamics in Boiling Under High Heat Flux Pulse Heating. Journal of Heat Transfer, Vol.113, November 1991.

Asai, A. Three-Dimensional Calculation of Bubble Growth and Drop Ejection in a Bubble Jet Printer. Journal of Fluids Engineering, Vol.114, December 1992.

Bhaskar E, Aden J. Development of the Thin-Film Structure for the Thinkjet Printhead. Hewlett Packard Journal, May 1985, pp. 27-33.

Bohorquez J, et al. Laser-Comparable Inkjet Text Printing. Hewlett Packard Journal, February 1994, pp. 9-17.

Box G, Behnken D. Some New Three Level Designs for the Study of Quantitative Variables. Technometrics, Vol. 2, No. 4. Nov. 1960.

Bromley, A.L. Heat Transfer in Stable Film Boiling. Chemical Engineering Progress, Vol. 46, 1950, pp. 221-227.

Carslaw H.S., Jaeger J.C. Conduction of Heat in Solids. Clarendon Press. Oxford. 1959.

Clark, B. Personal Communication. Hewlett Packard. 1996.

Douglas J. Alternating Direction Methods for Three Space Variables. Numerische Mathematik, Vol 4, 1962, pp. 41-63.

Elger, D. An Experimental and Analytical Study of the Internal Fluid Dynamics of an Inkjet Printhead. Ph.D. Thesis, Oregon State University. Corvallis, OR. 1986.

Florschuetz L, Chao B. On the Mechanics of Vapor Bubble Collapse. Journal of Heat Transfer, May 1965, pp. 209-220.

Hoffman J. Numerical Methods for Engineers and Scientists. McGraw Hill. New York. 1992.

Knight, Bill. Computer Modeling of a Thermal Inkjet Device. IS&T's Seventh International Congress on Advances in Non-Impact Printing Technologies, Vol. 1, October 6-11, 1991.

Knight, Bill. Personal Communication. Hewlett Packard. 1996.

Michaels A. Nucleation Phenomena. American Chemical Society. Washington D.C. 1966.

Olson H. Elements of Acoustical Engineering. D. Van Nostrand Company. New York. 1947.

Patzer J, Hofer E, Beurer G. Simulation of the Influence of Different Liquids for Inkjets under the Aspect of Color Printing. SPIE, Vol. 2171. 1994.

Plesset M, Zwick S. The Growth of Vapor Bubbles in Superheated Liquids. Journal of Applied Physics, Vol. 25, Num 4. April 1954.

Runge W. Berechnungsmodell Thermischer Tintenschreibwerke. VDI-Verlag, Reihe 1, Nr. 219. 1993 (in German).

Spiegel, M. Mathematical Handbook of Formulas and Tables. McGraw-Hill. New York. 1968.

Walker K.P., Freed A.D. Asymptotic Integration Algorithms for Nonhomogeneous, Nonlinear, First Order, Ordinary Differential Equations. NASA Technical Memorandum 103793. March 1991.